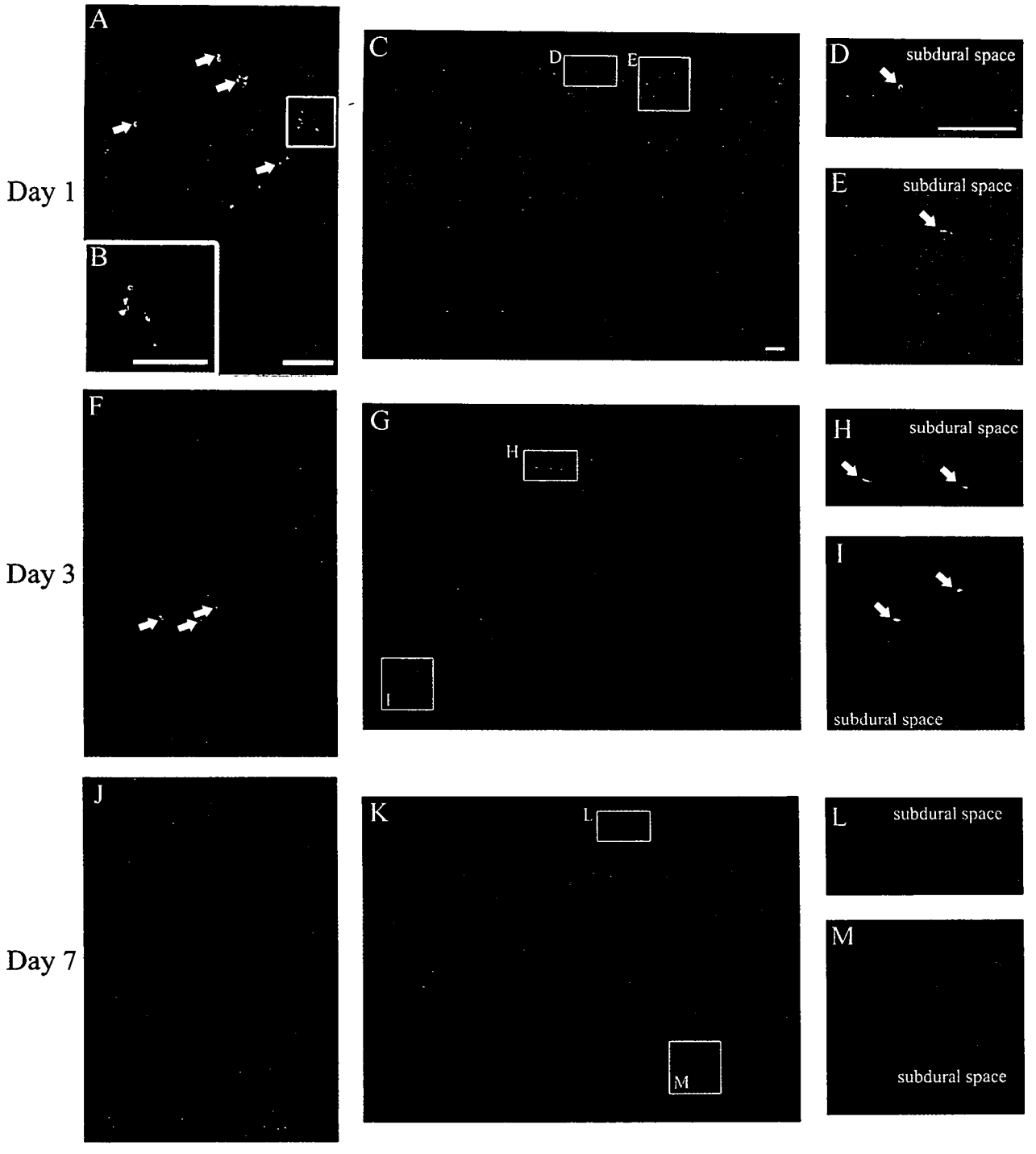

FIG. 2. Transplanted BM-MNC (arrows) were observed in the fourth ventricle and around the site of spinal cord injury (sagittal section). (**A–E**) On day 1 after transplantation, BM-MNC, labeled with PKH67 (green fluorescence), were observed very close to the choroid plexus in the ventricle (B is a magnified view of the box in A). Some transplanted cells became attached to the surface of the pia mater of the injured spinal cord (D and E are magnified views of the boxes in C). (**F–I**) On day 3, a few transplanted cells were seen in the ventricle (F), and some transplanted cells were integrated into the pia mater of the injured cord (H and I are magnified views of the boxes in G). (**J–M**) On day 7, almost no PKH67-labeled cells were observed (L and M are magnified views of the boxes in K). Nuclei were stained with TO-PRO-3 (blue). Scale bar = 100 μm (A–D).

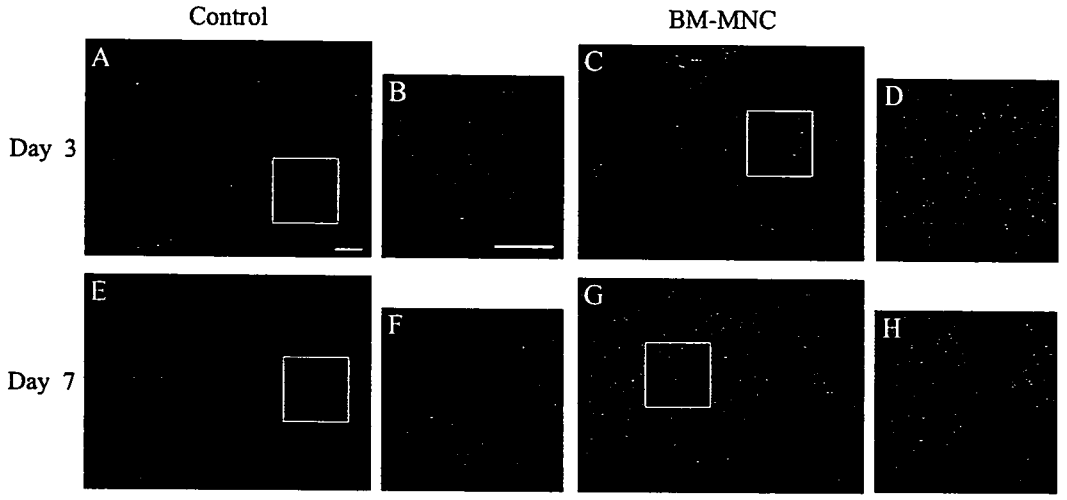

FIG. 4. Blood vessels stained for vWF at the site of SCI in the acute stage of injury. Immunohistochemical analysis of vWF (red) was performed on sagittal sections at the site of injury on day 3 (**A–D**) and day 7 (**E–H**) in animals treated with HBSS (A,B,E,F) or BM-MNC (C,D,G,H). Nuclei were stained with TO-PRO-3 (blue). vWF-positive cells were identified mainly around the center of the injured spinal cord (A–H). The figures in the right column (B,D,F,H) are magnified views of the boxes in A, C, E, and G, respectively. Scale bar = 200 μm (A,B).

TUNEL assays on sections obtained from the injury site on day 3 (Fig. 3E,F) after injury. TUNEL-positive (green) cells were observed mainly around the tissue not stained for β-tubulin type III at the injury site. The number of TUNEL-positive cells per high-power field (hpf) was significantly lower in BM-MNC-transplanted rats than in control rats (Fig. 3G). Consistent with these findings was a significantly higher density of nerve fibers stained for β-tubulin type III in BM-MNC-transplanted rats than in control rats (Fig. 3H).

To evaluate distribution of blood vessels at the site of injury, we performed immunohistochemistry for vWF on sections obtained on day 3 (Fig. 4A–D) and day 7 (Fig. 4E–H) after SCI. vWF-positive cells (red) were distributed mainly around the center of the injured spinal cord. Quantitative analysis revealed no significant difference between BM-MNC-transplanted rats and control rats in the density of vWF-positive cells at the injury site on day 7 (9.84 ± 0.83 vs. 10.8 ± 1.64 cells/mm^2, respectively; $p = 0.34$).

Increase in Hepatocyte Growth Factor Concentration in CSF with BM-MNC Transplantation

On day 3 after SCI, we obtained CSF and measured the concentrations in it of VEGF, HGF, and TNF-α by ELISA. The concentration of VEGF, a well-known an-

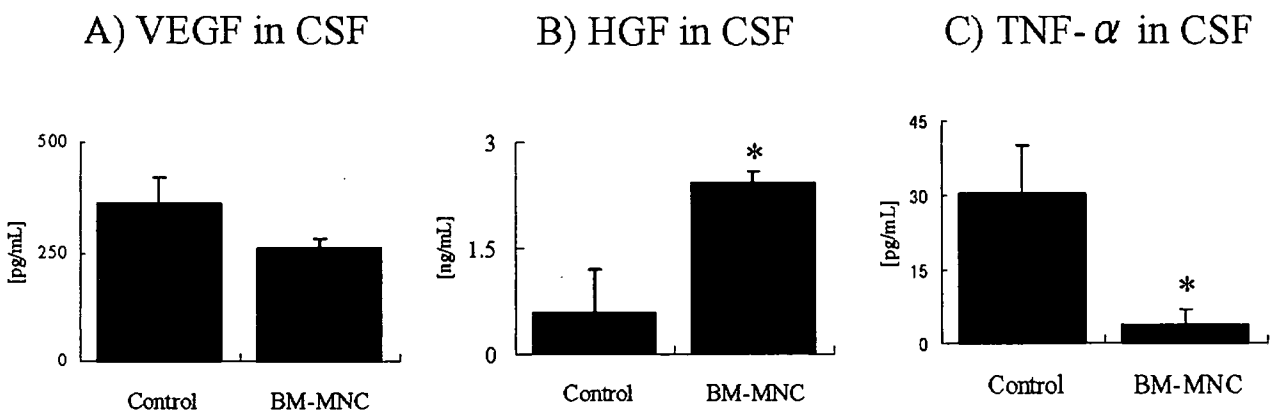

FIG. 5. Determination of concentrations of cytokines in CSF by ELISA. CSF was obtained from rats on day 3 after SCI. No significant difference was found in the concentration of VEGF in BM-MNC-transplanted and control animals (**A**). However, the concentration of HGF was remarkably higher in CSF from BM-MNC-transplanted rats than in that of control rats (**B**). A lower concentration of TNF-α was observed in the CSF of BM-MNC-transplanted than in that of control rats (**C**) ($n = 3$ per group). *$p < 0.05$ versus control.

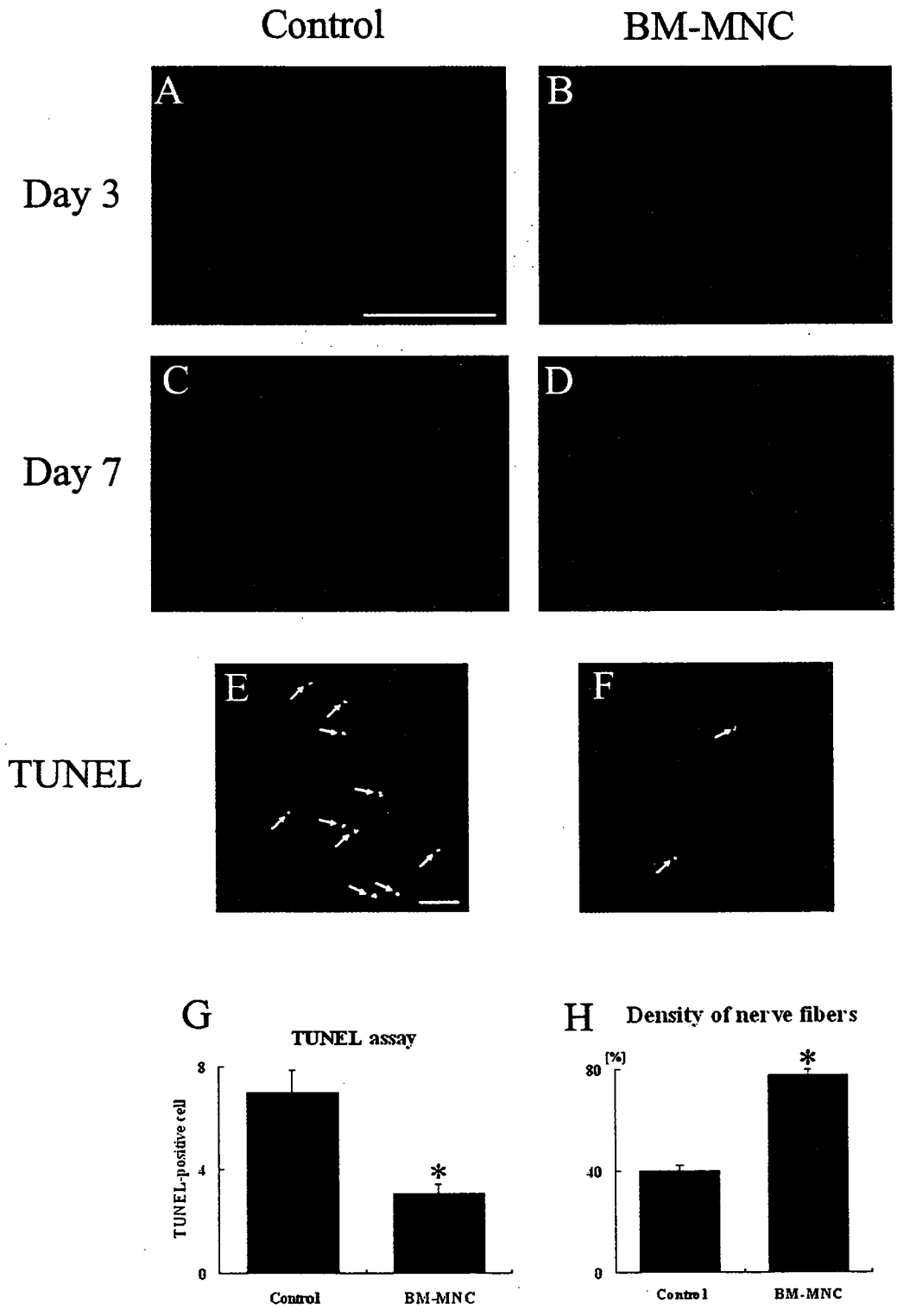

FIG. 3. Administration of BM-MNC reduced the number of apoptotic cells at the site of injury in the acute stage. (**A–D**) Sagittal sections obtained from the injury site on day 3 (A,B) and day 7 (C,D) were stained for β-tubulin type III. Axons stained for β-tubulin type III were preserved at the site of injury in BM-MNC-transplanted (B,D) compared to control rats (A,C). (**E,F**) TUNEL of fragmented DNA was performed on sagittal sections obtained on day 3 from the injury sites of control rats (E) and BM-MNC-transplanted rats (F). TUNEL-positive nuclei (green) were merged with cell nuclei (blue) as indicated by arrows. (**G**) The number of TUNEL-positive cells was significantly smaller in BM-MNC-transplanted than in control rats ($n = 3$ per group). $^*p < 0.01$ versus control. (**H**) The density of nerve fibers at the site of injury on day 7 was significantly higher in BM-MNC-transplanted than in control rats ($n = 3$ per group). $^*p < 0.05$ versus control. Scale bar = 1 mm (A), 50 μm (E).

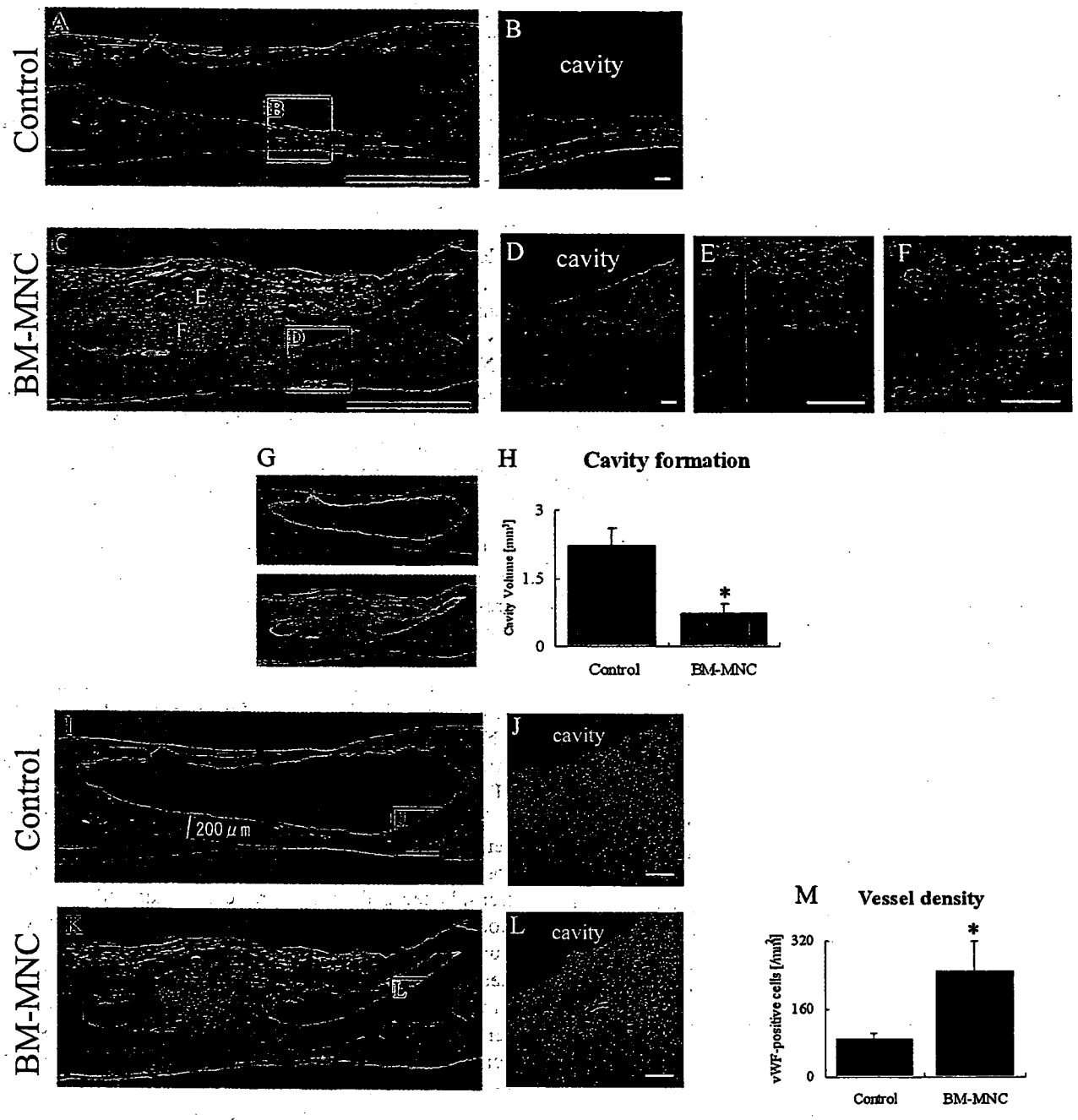

FIG. 6. Injured spinal cord on day 35 after SCI. (**A–H**) Although clear cavity formation was observed at the site of injury in control rats (A, H&E staining; B, staining for β-tubulin type III), only limited cavity formation was observed in BM-MNC-transplanted rats (C, H&E staining; D, staining for β-tubulin type III). Expression of β-tubulin type III (E) and GFAP (F) was confirmed in the tissue around the cavity. The area of the cavity was measured as indicated by yellow in G (H&E staining) in consecutive sagittal sections, and the volume of the cavity was calculated. A significant reduction in the cavity volume was found in BM-MNC-transplanted rats as compared to control rats (H; $n = 8$ per group). *$p = 0.01$ versus control. (**I–M**) Blood vessels stained for vWF (red) were observed in the marginal zone of the cavities of control rats (I,J) and BM-MNC-transplanted rats (K,L). The density of vWF-positive cells in the marginal zone, indicated by blue (I,K), was significantly increased in BM-MNC-transplanted as compared to control rats (M; $n = 8$). *$p < 0.05$ versus control. Scale bar = 1 mm (A,C), 100 μm (B,D–F,J,L).

giogenic factor (Carmeliet, 2003), did not show a significant increase with BM-MNC transplantation (Fig. 5A). This result was consistent with our finding that, in the acute stage of injury, there was no increase in the number of cells stained for vWF as a vascular marker. In contrast, we observed a remarkable increase in the concentration of HGF, which is known to have neuroprotective effects *in vivo* and *in vitro* (Tsuzuki et al., 2000; Zhang et al., 2000), with BM-MNC transplantation (Fig. 5B). These results may explain the decrease in concentration of TNF-α with BM-MNC transplantation (Fig. 5C).

Prevention of Cavity Formation in the Chronic Stage

To investigate whether BM-MNC have an inhibitory effect on degeneration of the injured spinal cord in the chronic stage of injury, we conducted a histologic study on sections obtained from the injury site on day 35 after SCI. SCI is known to cause secondary injury accompanied by inflammation, followed by cavity formation (Zhang and Guth, 1997). On day 35, clear cavity formation was observed in control rats (Fig. 6A, H&E staining; Fig. 6B, staining for β-tubulin type III). The cavity wall was composed of loosely packed tissue surrounded by numerous empty spaces, with cell nuclei sparsely dispersed throughout the wall. In contrast, limited cavity formation was observed with administration of BM-MNC (Fig. 6C, H&E staining; Fig. 6D, staining for β-tubulin type III). The wall of the cavity, composed of well-packed tissue as in the normal spinal cord, contained many cell nuclei. Tissue around the cavity was stained for β-tubulin type III (Fig. 6E) and GFAP (Fig. 6F). We determined the volume of the cavity at the site of injury by measuring the cavity area in sagittal cross sections (Fig. 6G). The volume of the cavity was significantly reduced in the BM-MNC-transplanted rats as compared with that in the control group (Fig. 6H). Moreover, many cells in the area immediately around the cavity stained for vWF (red), a marker of blood vessels (Fig. 6I–L). In the chronic stage of injury, the density of vWF-positive cells just around the cavity was significantly greater in BM-MNC-transplanted rats (Fig. 6K,L) than in control rats (Fig. 6I,J), as shown in Figure 6M.

DISCUSSION

We found that transplantation of BM-MNC soon after SCI had a neuroprotective effect in the acute stage of injury, promoting functional improvement, which was followed by the suppression of cavity formation.

In the acute stage of SCI, transplantation of BM-MNC protected nerve fibers of the injured spinal cord. Although the exact mechanism by which transplantation of BM-MNC exerts a therapeutic effect is unclear, our results indicate little contribution from VEGF; transplantation of BM-MNC did not significantly increase the VEGF concentration in CSF or promote angiogenesis at the site of injury in the acute stage. In contrast, a remarkable increase in the concentration of HGF in CSF was observed with BM-MNC transplantation. HGF is reported to be secreted by BM-MNC (Liu et al., 2004) and to have a strong antiapoptotic effect in neural injury (Tsuzuki et al., 2000; Zhang et al., 2000). These observations, in addition to the secretion by BM-MNC of other neuroprotective cytokines (Kamihata et al., 2001; Chen et al., 2002; Valable et al., 2003), at least partly explain the beneficial effects observed with BM-MNC transplantation. These neuroprotective effects may also explain the decrease in TNF-α concentration in CSF with transplantation of BM-MNC.

Cavity formation is a characteristic of progressive tissue necrosis, which follows the initial primary cell destruction in injury to the CNS (Zhang and Guth, 1997). Regulating injury in the acute stage has been reported to be the critical factor for controlling the progression of secondary injury to the CNS in SCI (Fitch et al., 1999), and in our study the neuroprotective effect of BM-MNC in the acute stage of injury contributed mainly to suppressing cavity formation in the chronic stage of SCI. In accord with these findings was the observed preservation of blood vessels in the chronic stage of injury with transplantation of BM-MNC. As previously reported, blood vessel formation is essential for the repair of tissue after CNS injury such as SCI (Imperato-Kalmar et al., 1997), brain trauma (Giulian et al., 1989), and brain infarction (Taguchi et al., 2004).

In the present study, no transplanted cells were observed in the injured spinal cord on day 7 after BM-MNC transplantation, indicating that the differentiation of transplanted cells into neural cells made little contribution to the positive effect of transplantation, at least with our protocol. Koshizuka et al. reported that immature hematopoietic stem cells from bone marrow, transplanted in the subacute stage of SCI (at 7 days after injury), differentiate into neural precursor cells, which may result in functional recovery partly through neurogenesis (Koshizuka et al., 2004). It has been shown that stem cell transplantation can improve neurologic function by several mechanisms, some of which are neuroprotective effects on host neurons from trophic factors secreted by transplanted cells, and/or the reestablishment of functional neural networks through the integration of transplanted cells (Lindvall and Kokaia, 2004). These observations suggest at least two critical mechanisms by which BM-MNC transplantation may promote functional re-

covery: neuroprotection, when the BM-MNC are transplanted in the hyperacute stage, and differentiation into neural cells, when BM-MNC are transplanted in the subacute stage.

Besides being studied in animal models of various diseases (Kamihata et al., 2001; Shintani et al., 2001), transplantation of BM-MNC has been investigated for effects on acute tissue injury, with promising results (Assmus et al., 2002; Tateishi-Yuyama et al., 2002). BM-MNC transplantation via the CSF after SCI has several advantages over other kinds of cell therapies, including those that use neural stem cells or embryonic stem cells. Furthermore, although transplantation of embryonic stem cells and neural precursor cells is reported to induce recovery from SCI (McDonald et al., 1999; Ogawa et al., 2002), some unresolved critical issues (i.e., ethical concerns and immunosuppression) have prevented its clinical application.

Clinical transplantation of BM-MNC via the CSF may be realized earlier than transplantation of these other types of cells. BM-MNC are easily collected and can be transplanted at the most appropriate time after SCI without sacrificing the time window critical for a therapeutic effect, and there is no need to expand BM-MNC by culture to obtain a sufficient number of cells for transplantation. Moreover, in the clinical setting, BM-MNC can be transplanted via the CSF by means of lumbar puncture rather than having to be given by ventricular injection, thereby reducing the risk of additional injury to intact spinal cord at the injury site.

In conclusion, transplantation of BM-MNC after SCI has a remarkable neuroprotective effect in the acute stage of injury, suppresses cavity formation, and contributes to functional recovery. Our observations provide evidence that clinical administration of BM-MNC can play a critical role in neuroprotection and new vessel formation for functional recovery after SCI, and we conclude that transplantation of BM-MNC after SCI is a potentially effective means of enhancing functional recovery from such injury.

ACKNOWLEDGMENTS

We are grateful to Associate Professors Hiroshi Tanaka and Takeshi Shimazu for their helpful advice, and we thank all of the members of our laboratory for critical discussion pertaining to the experiments done in the present study. This work was supported in part by the Ministry of Education, Science, Sports and Culture of Japan (grant 15300114), and the Ministry of Health, Labour and Welfare of Japan (grant 16C-7, H18-Kokoro-024).

REFERENCES

ASSMUS, B., SCHACHINGER, V., TEUPE, C., et al. (2002). Transplantation of progenitor cells and regeneration enhancement in acute myocardial infarction (TOPCARE-AMI). Circulation **106,** 3009–3017.

AZIZI, S.A., STOKES, D., AUGELLI, B.J., et al. (1998). Engraftment and migration of human bone marrow stromal cells implanted in the brains of albino rats—similarities to astrocyte grafts. Proc. Natl. Acad. Sci. USA **95,** 3908–3913.

BAI, H., SUZUKI, Y., NODA, T., et al. (2003). Dissemination and proliferation of neural stem cells on the spinal cord by injection into the fourth ventricle of the rat: a method for cell transplantation. J. Neurosci. Methods **124,** 181–187.

BASSO, D.M., BEATTIE, M.S., and BRESNAHAN, J.C. (1995). A sensitive and reliable locomotor rating scale for open field testing in rats. J. Neurotrauma **12,** 1–21.

CARMELIET, P. (2003). Angiogenesis in health and disease. Nat. Med. **9,** 653–660.

CHEN, X., KATAKOWSKI, M., LI, Y., et al. (2002). Human bone marrow stromal cell cultures conditioned by traumatic brain tissue extracts: growth factor production. J. Neurosci. Res. **69,** 687–691.

DOUCETTE, R. (1995). Olfactory ensheathing cells: potential for glial cell transplantation into areas of CNS injury. Histol. Histopathol. **10,** 503–507.

FITCH, M.T., DOLLER, C., COMBS, C.K., et al. (1999). Cellular and molecular mechanisms of glial scarring and progressive cavitation: *in vivo* and *in vitro* analysis of inflammation-induced secondary injury after CNS trauma. J. Neurosci. **19,** 8182–8198.

GIULIAN, D., CHEN, J., INGEMAN, J.E., GEORGE, J.K., and NOPONEN, M. (1989). The role of mononuclear phagocytes in wound healing after traumatic injury to adult mammalian brain. J. Neurosci. **9,** 4416–4429.

IDE, C., KITADA, M., CHAKRABORTTY, S., et al. (2001). Grafting of choroid plexus ependymal cells promotes the growth of regenerating axons in the dorsal funiculus of rat spinal cord: a preliminary report. Exp. Neurol. **167,** 242–251.

IMPERATO-KALMAR, E.L., McKINNEY, R.A., SCHNELL, L., et al. (1997). Local changes in vascular architecture following partial spinal cord lesion in the rat. Exp. Neurol. **145,** 322–328.

KAMIHATA, H., MATSUBARA, H., NISHIUE, T., et al. (2001). Implantation of bone marrow mononuclear cells into ischemic myocardium enhances collateral perfusion and regional function via side supply of angioblasts, angiogenic ligands, and cytokines. Circulation **104,** 1046–1052.

KONDZIOLKA, D., WECHSLER, L., GOLDSTEIN, S., et al. (2000). Transplantation of cultured human neuronal cells for patients with stroke. Neurology **55,** 565–569.

KOSHIZUKA, S., OKADA, S., OKAWA, A., et al. (2004). Transplanted hematopoietic stem cells from bone marrow differentiate into neural lineage cells and promote functional recovery after spinal cord injury in mice. J. Neuropathol. Exp. Neurol. **63,** 64–72.

LINDVALL, O., and KOKAIA, Z. (2004). Recovery and rehabilitation in stroke: stem cells. Stroke **35,** 2691–2694.

LIU, Y., GUO, J., ZHANG, P., et al. (2004). Bone marrow mononuclear cell transplantation into heart elevates the expression of angiogenic factors. Microvasc. Res. **68,** 156–160.

MARTIN, D., ROBE, P., FRANZEN, R., et al. (1996). Effects of Schwann cell transplantation in a contusion model of rat spinal cord injury. J. Neurosci. Res. **45,** 588–597.

McDONALD, J.W., LIU, X.Z., QU, Y., et al. (1999). Transplanted embryonic stem cells survive, differentiate and promote recovery in injured rat spinal cord. Nat. Med. **5,** 1410–1412.

OGAWA, Y., SAWAMOTO, K., MIYATA, T., et al. (2002). Transplantation of *in vitro*-expanded fetal neural progenitor cells results in neurogenesis and functional recovery after spinal cord contusion injury in adult rats. J. Neurosci. Res. **69,** 925–933.

OHTA, M., SUZUKI, Y., NODA, T., et al. (2004). Bone marrow stromal cells infused into the cerebrospinal fluid promote functional recovery of the injured rat spinal cord with reduced cavity formation. Exp. Neurol. **187,** 266–278.

REHMAN, J., LI, J., ORSCHELL, C.M., and MARCH, K.L. (2003). Peripheral blood "endothelial progenitor cells" are derived from monocyte/macrophages and secrete angiogenic growth factors. Circulation **107,** 1164–1169.

REYES, M., and VERFAILLIE, C.M. (2001). Characterization of multipotent adult progenitor cells, a subpopulation of mesenchymal stem cells. Ann. N.Y. Acad. Sci. **938,** 231–235.

SHINTANI, S., MUROHARA, T., IKEDA, H., et al. (2001). Augmentation of postnatal neovascularization with autologous bone marrow transplantation. Circulation **103,** 897–903.

STRAUER, B.E., BREHM, M., ZEUS, T., et al. (2002). Repair of infarcted myocardium by autologous intracoronary mononuclear bone marrow cell transplantation in humans. Circulation **106,** 1913–1918.

TAGUCHI, A., SOMA, T., TANAKA, H., et al. (2004). Administration of $CD34^+$ cells after stroke enhances neurogenesis via angiogenesis in a mouse model. J. Clin. Invest. **114,** 330–338.

TAKAMI, T., OUDEGA, M., BETHEA, J.R., et al. (2002). Methylprednisolone and interleukin-10 reduce gray matter damage in the contused Fischer rat thoracic spinal cord but do not improve functional outcome. J. Neurotrauma **19,** 653–666.

TATEISHI-YUYAMA, E., MATSUBARA, H., MUROHARA, T., et al. (2002). Therapeutic angiogenesis for patients with limb ischaemia by autologous transplantation of bone-marrow cells: a pilot study and a randomised controlled trial. Lancet **360,** 427–435.

TOMITA, M., ADACHI, Y., YAMADA, H., et al. (2002). Bone marrow–derived stem cells can differentiate into retinal cells in injured rat retina. Stem Cells **20,** 279–283.

TSUZUKI, N., MIYAZAWA, T., MATSUMOTO, K., et al. (2000). Hepatocyte growth factor reduces infarct volume after transient focal cerebral ischemia in rats. Acta Neurochir. Suppl. **76,** 311–316.

VALABLE, S., BELLAIL, A., LESNE, S., et al. (2003). Angiopoietin-1–induced PI3-kinase activation prevents neuronal apoptosis. FASEB J. **17,** 443–445.

WIDENFALK, J., LIPSON, A., JUBRAN, M., et al. (2003). Vascular endothelial growth factor improves functional outcome and decreases secondary degeneration in experimental spinal cord contusion injury. Neuroscience **120,** 951–960.

WU, S., SUZUKI, Y., EJIRI, Y., et al. (2003). Bone marrow stromal cells enhance differentiation of cocultured neurosphere cells and promote regeneration of injured spinal cord. J. Neurosci. Res. **72,** 343–351.

ZHANG, Z., and GUTH, L. (1997). Experimental spinal cord injury: Wallerian degeneration in the dorsal column is followed by revascularization, glial proliferation, and nerve regeneration. Exp. Neurol. **147,** 159–171.

ZHANG, L., HIMI, T., MORITA, I., and MUROTA, S. (2000). Hepatocyte growth factor protects cultured rat cerebellar granule neurons from apoptosis via the phosphatidylinositol-3 kinase/Akt pathway. J. Neurosci. Res. **59,** 489–496.

Address reprint requests to:
Tomoyuki Yoshihara, M.D.
Department of Traumatology
and Acute Critical Medicine
Osaka University Graduate School of Medicine
2-15 Yamadaoka, Suita
Osaka 565-0871, Japan

E-mail: t-yoshihara@umin.ac.jp

European Journal of Neuroscience, Vol. 26, pp. 126–133, 2007 doi:10.1111/j.1460-9568.2007.05640.x

Granulocyte colony-stimulating factor has a negative effect on stroke outcome in a murine model

Akihiko Taguchi,[1] Zhongmin Wen,[1] Kazunori Myojin,[1] Tomoyuki Yoshihara,[1] Takayuki Nakagomi,[2] Daisuke Nakayama,[1] Hidekazu Tanaka,[3] Toshihiro Soma,[4] David M. Stern,[5] Hiroaki Naritomi[1] and Tomohiro Matsuyama[2]

[1]Department of Cerebrovascular Disease, National Cardiovascular Center, 5-7-1 Fujishiro-dai, Suita, Osaka, Japan, 565-8565
[2]Department of Advanced Medicine, Hyogo College of Medicine, Hyogo, Japan
[3]Department of Pharmacology, Graduate School of Medicine, Osaka University, Osaka, Japan
[4]Department of Hematology, Osaka Minami National Hospital, Osaka, Japan
[5]Dean's Office, College of Medicine, University of Cincinnati, OH, USA

Keywords: angiogenesis, cerebral infarction, inflammation, neuroprotection

Abstract

The administration of CD34-positive cells after stroke has been shown to have a beneficial effect on functional recovery by accelerating angiogenesis and neurogenesis in rodent models. Granulocyte colony-stimulating factor (G-CSF) is known to mobilize CD34-positive cells from bone marrow and has displayed neuroprotective properties after transient ischemic stress. This led us to investigate the effects of G-CSF administration after stroke in mouse. We utilized permanent ligation of the M1 distal portion of the left middle cerebral artery to develop a reproducible focal cerebral ischemia model in CB-17 mice. Animals treated with G-CSF displayed cortical atrophy and impaired behavioral function compared with controls. The negative effect of G-CSF on outcome was associated with G-CSF induction of an exaggerated inflammatory response, based on infiltration of the peri-infarction area with CD11b-positive and F4/80-positive cells. Although clinical trials with G-CSF have been started for the treatment of myocardial and limb ischemia, our results indicate that caution should be exercised in applying these results to cerebral ischemia.

Introduction

Granulocyte colony-stimulating factor (G-CSF) was identified in 1975 and has been broadly used for mobilizing granulocytes from bone marrow (Weaver *et al.*, 1993). G-CSF is also known to mobilize immature hematopoietic cells that include endothelial progenitor cells (EPCs) (Willing *et al.*, 2003). In view of the capacity of circulating EPCs to enhance neovascularization of ischemic tissues (Asahara *et al.*, 1997), the results of recent studies demonstrating that infusion of EPCs accelerates angiogenesis at ischemic sites, thereby limiting tissue injury, is not unexpected (Dzau *et al.*, 2005). As a potential extension of this concept, administration of G-CSF has been shown to accelerate angiogenesis in animal models of limb and myocardial ischemia (Minatoguchi *et al.*, 2004). These observations have provided a foundation for clinical trials testing the effects of G-CSF in limb and myocardial ischemia (Kuethe *et al.*, 2004).

Stroke, a critical ischemic disorder in which there are important opportunities for neuroprotective therapies, is another situation in which enhanced angiogenesis might be expected to improve outcome. For example, we have shown that the administration of CD34-positive cells after stroke accelerates angiogenesis and, subsequently, neurogenesis (Taguchi *et al.*, 2004). Similarly, erythropoietin (EPO), also known to have angiogenic properties, has been shown to have beneficial effects in experimental cerebral ischemia (Ehrenreich *et al.*, 2002; Wang *et al.*, 2004). In addition, G-CSF displays neuroprotective properties *in vitro* (Schabitz *et al.*, 2003) and *in vivo* (Schabitz *et al.*, 2003; Shyu *et al.*, 2004; Gibson *et al.*, 2005), the latter in a rodent model of transient cerebral ischemic damage. Models of transient cerebral ischemia allow subtle assessment of neuroprotective properties, such as the survival of vulnerable neuronal populations in the penumbra. However, functional outcome after stroke is also determined by inflammation and reparative processes consequent to extensive brain necrosis, the latter better modelled by permanent cerebral ischemia. We have evaluated the effect of G-CSF on stroke outcome in a model of permanent cerebral ischemia with massive cell necrosis. Our model employs permanent ligation of the left middle cerebral artery (MCA) and results in extensive neuronal death in the ischemic zone, as well as more selective apoptotic cell death in the penumbral area (Walther *et al.*, 2002). Using this model, we have tested the effect of G-CSF on functional recovery after stroke.

Materials and methods

All procedures were performed under the auspices of an approved protocol of the Japanese National Cardiovascular Center Animal Care and Use Committees (protocol no. 06026, approval date, May 22, 2006).

Induction of focal cerebral ischemia

To assess the effect of G-CSF on stroke, we developed a highly reproducible murine stroke model applying our previous method

Correspondence: Dr Akihiko Taguchi, as above.
E-mail: ataguchi@res.ncvc.go.jp

Received 19 October 2006, revised 25 April 2007, accepted 21 May 2007

(Taguchi *et al.*, 2004) to CB-17 mice (Clea, Tokyo, Japan). Under halothane anesthesia (inhalation of 3%), the left zygoma was dissected to visualize the MCA through the cranial bone. A hole was made using a dental drill in the bone (diameter 1.5 mm) and the MCA was carefully isolated, electro-cauterized and disconnected just distal to its crossing of the olfactory tract (distal M1 portion). Cerebral blood flow in the MCA area was monitored as described previously (Matsushita *et al.*, 1998). Briefly, an acrylate column was attached to the intact skull using stereotactic coordinates (1 mm anterior and 3 mm lateral to the bregma) and cerebral blood flow was assessed using a linear probe (1 mm in diameter) by laser Doppler flowmetry (Neuroscience Co. Ltd, Osaka, Japan). Mice that showed decreased cerebral blood flow by ~75% immediately after the procedure were used for experiments (success rate of >95%). Body temperature was maintained at 36.5–37 °C using a heat lamp (Nipponkoden, Tokyo, Japan) during the operation and for 2 h after MCA occlusion. At later timepoints, mice were first subjected to behavioral tests and then to histological examination of their brains. For histological examination, mice were perfusion-fixed with 100 mL of periodate-lysine-paraformaldehyde fixative under deep (pentobarbital) anesthesia (100 mg/kg, intraperitonealy) and their brains were removed. Coronal brain sections (20 μm) were cut on a vibratome (Leica, Solms, Germany) and subjected to immunocytochemistry.

Administration of granulocyte colony-stimulating factor and erythropoietin following stroke

To examine the effect of G-CSF on ischemic cerebral injury, human recombinant G-CSF (Kirin, Tokyo, Japan) was administered subcutaneously at four doses (0.5, 5, 50 or 250 μg/kg) at 24, 48 and 72 h after induction of stroke. As controls, the same volume of phosphate-buffered saline (PBS) or recombinant human EPO (1000 μg/kg; Kirin), the latter known to have angiogenic properties and a positive effect on stroke outcome (Jaquet *et al.*, 2002), was administered subcutaneously. Other time courses of G-CSF administration, including 1 h after stroke (at doses of 0.5, 5, 50 or 250 μg/kg) and continuous administration (100 μg/kg/day) by micro-osmotic pump (Durect, Cupertino, CA, USA) started 1 h after stroke over 7 days, were also studied. To exclude possible effects of an immune response to human recombinant G-CSF in the mouse, murine recombinant G-CSF (R & D Systems, Minneapolis, MN, USA; doses of 0.5, 5 or 50 μg/kg) was administered subcutaneously at 24, 48 and 72 h after induction of stroke, as indicated.

Immunohistochemistry

To evaluate the inflammatory response following administration of G-CSF post-stroke, brain sections were studied immunohistochemically using antibody to CD11b (BD Biosciences, San Jose, CA, USA) and F4/80 (Serotec, Raleigh, NC, USA). The numbers of CD11b-positive inflammatory cells at the anterior cerebral artery (ACA)/MCA border of the infarcted area and numbers of F4/80-positive ($F4/80^+$) activated microglia/macrophages in the ACA area at the exact center of the forebrain section (at the midpoint of the left forebrain, as shown with an orange line in Fig. 1J) were scored by two investigators blinded to the experimental protocol.

Analysis of the peri-infarction and infarcted area after middle cerebral artery occlusion

To investigate mechanisms of brain damage/atrophy consequent to administration of G-CSF, neovessel formation and the extent of infarction were analysed. Formation of new vessels was assessed at the border of the MCA and ACA territories by perfusing carbon black (0.5 mL; Fuekinori, Osaka, Japan) via the left ventricle of the heart. Staining with 2,3,5-triphenyltetrazolium (TTC) (Sigma-Aldrich, St Louis, MO, USA) was employed to demarcate the border of viable/non-viable tissue. Semiquantitative analysis of angiogenesis employed an angiographic score. Briefly, microscopic digital images were scanned into a computer (Keyence, Osaka, Japan) and the number of carbon black-positive microvessels crossing the border zone of the TTC-negative MCA area to the TTC-positive ACA area was determined. To evaluate the infarcted area 3 days after stroke, coronal brain sections at the exact center of the forebrain were stained with TTC. The infarcted area was measured using a microscopic digital camera system (Olympus, Tokyo, Japan). Infarction in this stroke model was highly reproducible and limited to the left cortex. NIH IMAGE software was used to quantify the TTC-positive area in the ACA territory. A brain atrophy index was established using whole brain images captured by a digital camera system (Olympus). The length of the forebrain was measured along the x and y dimensions shown in Fig. 1J and the ratio of $x : y$ was defined as the brain atrophy index.

Behavioral analysis

To assess cortical function, mice were subjected to behavioral testing using the open field task (Kimble, 1968) at 35 days after stroke. In this behavioral paradigm, animals were allowed to search freely in a square acrylic box (30 × 30 cm) for 60 min. A light source on the ceiling of the enclosure was on during the first 30 min (light period) and was turned off during a subsequent 30-min period. On the X- and Y-banks of the open field, two infrared beams were mounted 2 cm above the floor, spaced at 10 cm intervals, forming a flip–flop circuit between them. The total number of beam crossings by the animal was counted and scored as traveling behavior (locomotion). Twelve infrared beams were set 5 cm above the floor, spaced at 3 cm intervals, on the X-bank and the total number of beam crossings was counted and scored as rearing behavior (rearing). To exclude the contribution of physical deficits directly related to the operative procedure and induction of stroke, motor deficiencies were examined on day 35 after stroke. Neurological deficits were scored on a three-point modified scale as described previously (Tamatani *et al.*, 2001): 0, no neurological deficit; 1, failure to extend the left forepaw fully; 2, circling to left and 3, loss of walking or righting reflex. Body weight, monitored in each experimental group, displayed no significant differences (data not shown).

Data analysis

Statistical comparisons among groups were determined using one-way ANOVA and the Dunnett test was used for post-hoc analysis to compare with PBS controls. Where indicated, individual comparisons were performed using Student's t-test. In all experiments, mean ± SEM is reported.

Results

Induction of stroke in CB-17 mice

In a previous report, we demonstrated reproducible strokes in severe combined immunodeficient (SCID) mice by permanent ligation of the left MCA (Taguchi *et al.*, 2004). As SCID mice originated from the CB-17 strain, we expected anatomical similarity of cerebral arteries in

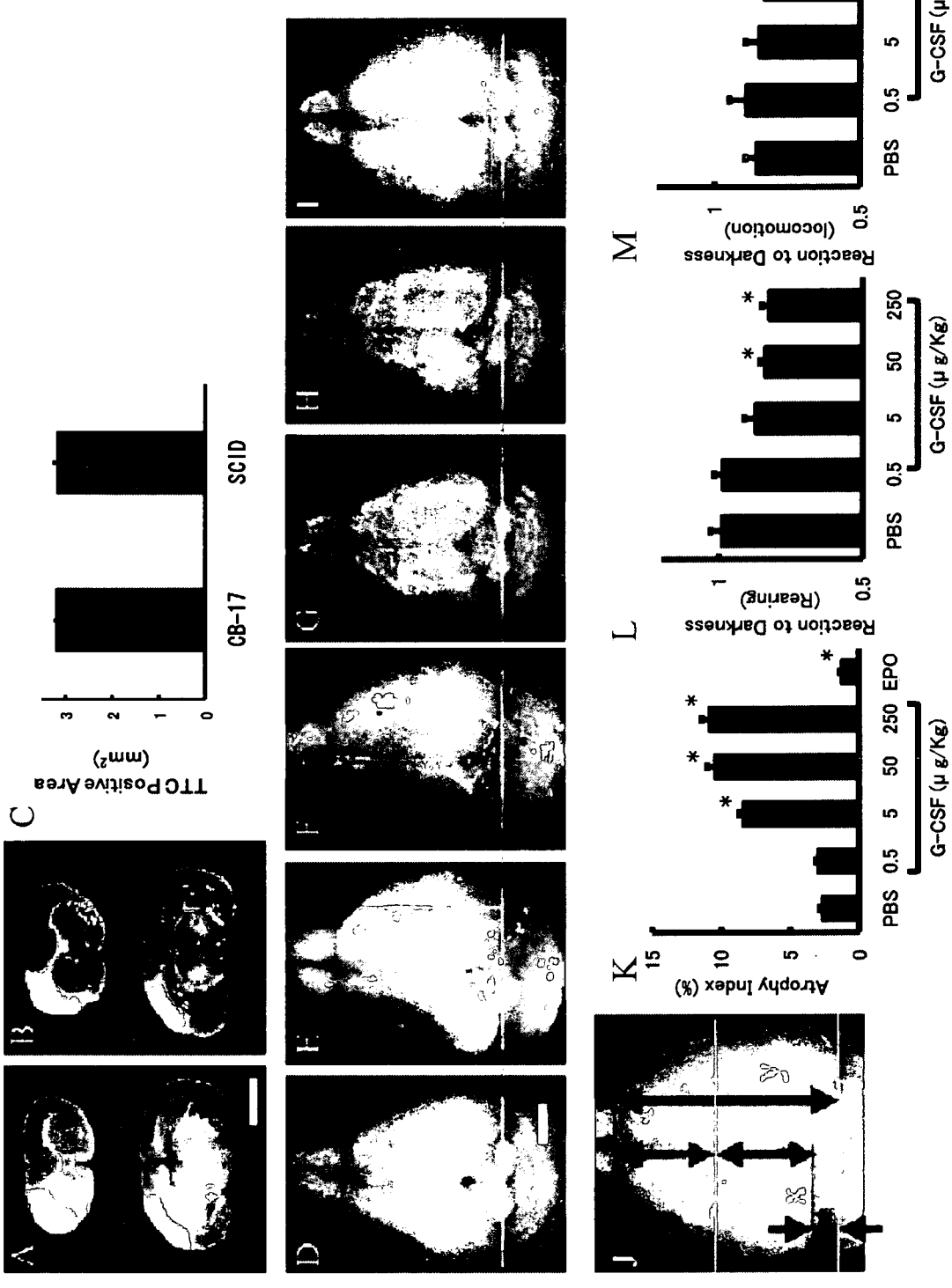

FIG. 1. Administration of granulocyte colony-stimulating factor (G-CSF) induces cortical atrophy. (A–C) Induction of stroke by ligation of the M1 portion of the left middle cerebral artery (MCA). Forebrain sections harvested from mice 3 h after stroke were stained with 2,3,5-triphenyltetrazolium (TTC), and lack of positive staining is observed in the MCA cortex of CB-17 (A) and severe combined immunodeficient (SCID) mice (B). The TTC-positive anterior cerebral artery area at the exact center of forebrain was quantified using NIH IMAGE (C). A highly reproducible TTC-positive (surviving) cortical area was observed in CB-17 and SCID mice. (D–I) On day 35 post-stroke, brains were evaluated grossly. Compared with post-stroke mice treated with phosphate-buffered saline (PBS) (D), no significant difference was observed in mice treated with 0.5 μg/kg of G-CSF (E). In contrast, brain atrophy was observed with G-CSF treatment at doses of 5 μg/kg (F), 50 μg/kg (G) or 250 μg/kg (H). Treatment with erythropoietin (EPO) (I) had a beneficial effect in terms of brain atrophy. Note that, compared with the contralateral side (green line), atrophy in the longitudinal direction was observed in animals treated with G-CSF (F–H). (J) A brain atrophy index was defined as the ratio of $x : y$. (K) ANOVA analysis ($n = 6$ per group) revealed significant brain atrophy in mice at doses of G-CSF above 0.5 μg/kg. In contrast, a reduction of brain atrophy was observed in mice treated with EPO. (L and M) Behavioral analysis post-stroke. ANOVA analysis ($n = 6$ per group) in mice subjected to stroke revealed that treatment with either 50 or 250 μg/kg of G-CSF significantly impaired the rearing response compared with PBS (L), although no significant difference was observed in locomotion (M). Marker bars, 2 mm (A and D). *$P < 0.05$ vs. PBS.

these two strains. Strokes were induced in CB-17 mice by permanent ligation of the M1 distal portion of the left MCA. To evaluate the infarcted area, brain sections were stained with TTC at 3 h after stroke. Reproducible strokes were induced in CB-17 mice (Fig. 1A) that were similar to those in SCID mice (Fig. 1B). The surviving cortical area post-stroke, represented by the TTC-positive ACA area at the exact center of forebrain, was also similar in CB-17 and SCID mice (Fig. 1C, $n = 6$/species).

Granulocyte colony-stimulating factor accelerates brain injury after stroke

In a previous study, we demonstrated that enhanced neovascularization post-stroke, due to administration of CD34-positive cells, promoted neuronal regeneration leading to cortical expansion and functional recovery (Taguchi *et al.*, 2004). As G-CSF is known to mobilize CD34-positive cells from bone marrow (Kuethe *et al.*, 2004), we investigated the effects of G-CSF treatment, starting 24 h after stroke and continuing for 3 days, using the above permanent focal cerebral ischemia model. Compared with control animals receiving PBS alone (Fig. 1D), no significant difference was observed in mice that received 0.5 μg/kg of G-CSF (Fig. 1E and K) at 35 days after stroke. However, remarkable brain atrophy was observed with G-CSF treatment at 5 μg/kg (Fig. 1F and K), 50 μg/kg (Fig. 1G and K) or 250 μg/kg (Fig. 1H and K). In contrast, a mild protective effect, with respect to brain atrophy, was observed in the group treated with EPO post-stroke (1000 μg/kg; Fig. 1I and K). In each condition depicted in Fig. 1, a representative image is shown and quantitative analysis of the brain atrophy index ($n = 6$/experimental condition; defined in Fig. 1J) is demonstrated in Fig. 1K.

Granulocyte colony-stimulating factor has a negative effect on functional recovery after stroke

To investigate functional recovery in animals treated with G-CSF, we performed behavioral testing on day 35 after stroke ($n = 6$, for each group). Compared with post-stroke CB-17 mice that received PBS, mice treated with 50 or 250 μg/kg G-CSF displayed impaired behavioral function as assessed by the 'dark' response, with respect to rearing (Fig. 1L and Table 1) analysed by ANOVA followed by post-hoc Dunnett test, although there was no significant change in locomotion (Fig. 1M). In contrast, treatment with EPO accelerated functional recovery with respect to both rearing (1.18 ± 0.07 and 0.99 ± 0.04 in EPO and PBS groups, respectively, $n = 6$ per group, $P < 0.05$) and locomotion (1.04 ± 0.04 and 0.85 ± 0.04 in EPO and PBS groups, respectively, $n = 6$ per group, $P < 0.05$). Mice showed rapid recovery from focal motor deficits and, by day 16 post-stroke, no motor deficits were detected based on a modified three-point scale (not shown).

Granulocyte colony-stimulating factor accelerates angiogenesis after stroke

Increased brain atrophy and impaired functional recovery in animals treated with G-CSF post-stroke were quite unexpected because of the known ability of G-CSF to mobilize CD34-positive cells from bone marrow (Willing *et al.*, 2003). In addition, a previous study showed neuroprotective properties of G-CSF in models of transient cerebral ischemia (Schabitz *et al.*, 2003). These considerations led us to analyse mechanisms contributing to increased brain atrophy after

TABLE 1. Raw data of open field test (G-CSF rearing)

Treatment and individual	Rearing (counts)		Reaction to darkness (Right OFF/Right ON)
	Right ON	Right OFF	
PBS			
1	662	640	0.97
2	611	708	1.16
3	487	450	0.92
4	587	540	0.92
5	482	430	0.89
6	425	450	1.06
Mean ± SEM	542.3 ± 37.2	536.3 ± 47.1	0.99 ± 0.04
G-CSF (0.5μg/kg)			
1	600	562	0.94
2	601	650	1.08
3	494	425	0.86
4	731	731	1.00
5	767	784	1.02
6	498	501	1.01
Mean ± SEM	615.2 ± 46.7	608.8 ± 56.2	0.98 ± 0.03
G-CSF (5μg/kg)			
1	577	497	0.86
2	537	368	0.69
3	310	288	0.93
4	520	485	0.93
5	673	652	0.97
6	572	480	0.84
Mean ± SEM	531.5 ± 49.3	461.7 ± 50.8	0.87 ± 0.04
G-CSF (50μg/kg)			
1	592	520	0.88
2	463	376	0.81
3	478	430	0.90
4	307	250	0.81
5	484	410	0.85
6	385	295	0.77
Mean ± SEM	451.5 ± 39.6	380.2 ± 39.6	0.84 ± 0.02
G-CSF (250μg/kg)			
	578	424	0.73
	501	401	0.80
	507	380	0.75
	465	412	0.89
	380	341	0.90
	401	347	0.87
Mean ± SEM	472 ± 29.9	384.2 ± 14.0	0.82 ± 0.03

Right ON, under light condition; Right OFF, under dark condition.

administration of G-CSF. As G-CSF has been reported to accelerate angiogenesis in limb and cardiac models of ischemic injury (Minatoguchi *et al.*, 2004), we sought to determine its impact on neovascularization in our permanent focal cerebral infarction model. Compared with PBS-treated controls (Fig. 2A), increased neovasculature at the border of the MCA and ACA cortex (staining with TTC demarcates viable/non-viable tissue and carbon black was used to visualize vessels) was observed in animals treated with G-CSF (50 μg/kg, Fig. 2B). Assessment of the angiographic score confirmed the impression of increased neovasculature in animals treated with G-CSF, compared with the group receiving PBS (Fig. 2C; $P < 0.05$).

Next, we investigated possible neuroprotective properties of G-CSF after stroke. Analysis of the infarcted/surviving area 3 days after stroke was evaluated in animals treated with PBS (Fig. 2D) or G-CSF (50 μg/kg, Fig. 2E) based on TTC staining; there was no effect of G-CSF treatment compared with controls receiving PBS (Fig. 2F). Thus, G-CSF did not impact on the viability of 'at-risk' tissue in the

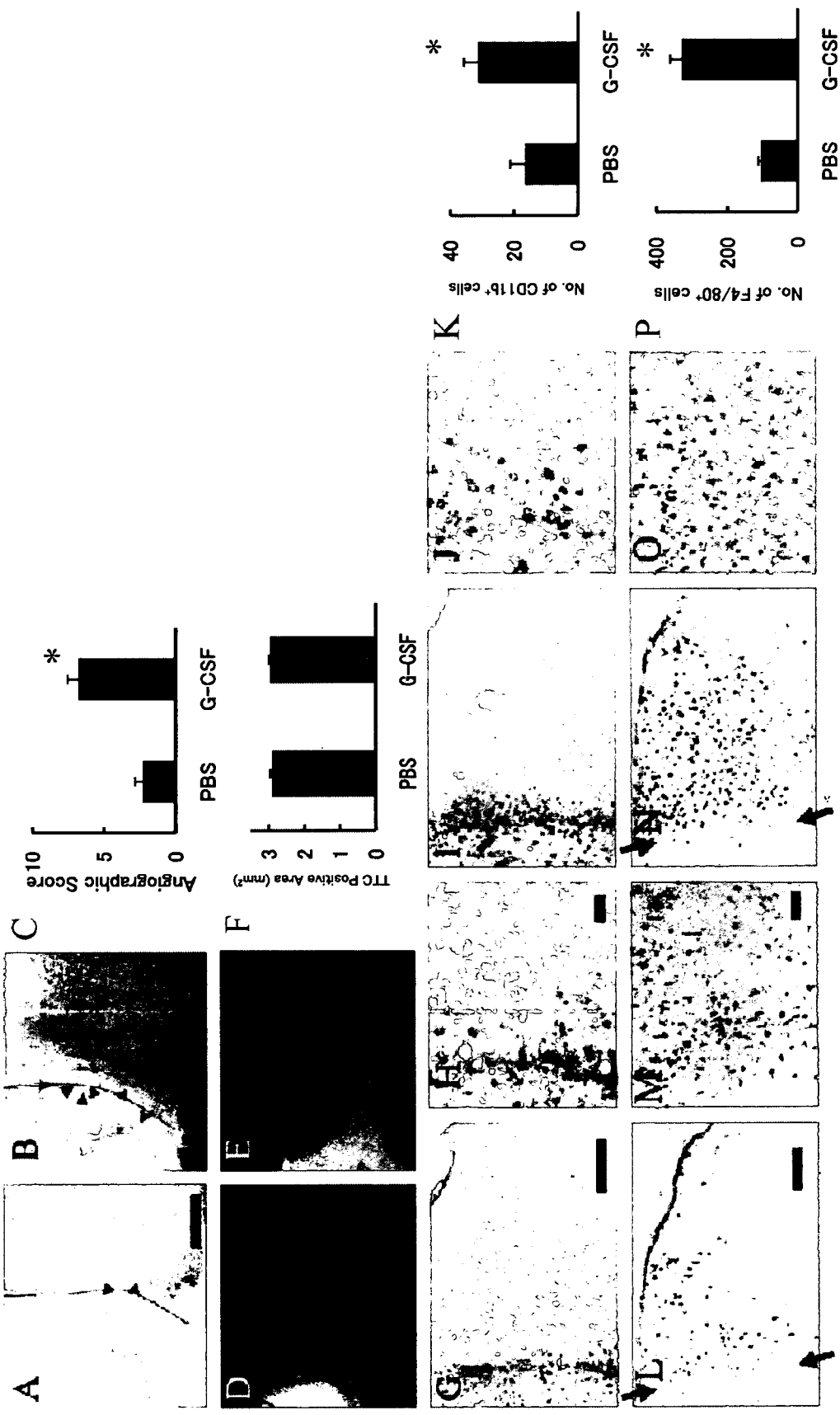

FIG. 2. Administration of granulocyte colony-stimulating factor (G-CSF) after stroke enhances the inflammatory response. (A–C) On day 3 after stroke, mice were infused with carbon black ink. Compared with mice treated with phosphate-buffered saline (PBS) (A), increased neovascularization was observed at the border between anterior cerebral artery (ACA) and middle cerebral artery (MCA) regions in mice treated with G-CSF (B). Representative micrographs are shown. The angiographic score (see Materials and methods) showed increased neovascularization ($n = 6$ per group) in mice treated with G-CSF post-stroke compared with controls (PBS). (D–F) There was no difference in the 2,3,5-triphenyltetrazolium (TTC)-positive ACA area at the exact center of forebrain comparing post-stroke animals treated with G-CSF (E) and controls/PBS (D). Sections from each animal were subjected to statistical analysis using Student's *t*-test ($n = 6$ animals per group; F). (G–K) CD11b-positive cells were visualized in the ACA area in tissue from post-stroke animals treated with PBS (G, lower magnification; H, higher magnification; I, lower magnification) or G-CSF (I, lower magnification; J, higher magnification). Sections from each animal were evaluated ($n = 6$ animals per group) and the average number of CD11b-positive cells per high power field is shown in each of the two groups (K). (L–P) F4/80-positive ($F4/80^+$) activated macrophages/microglia in mice treated with PBS were relatively limited to the area close to the border of infarcted tissue (L, lower magnification; M, higher magnification). However, an expanded area and increased density of $F4/80^+$ cells was observed after administration of G-CSF (N, lower magnification; O, higher magnification). The total number of $F4/80^+$ activated macrophages/microglia in the viable ACA area identified on the section at exact center of forebrain was quantified ($n = 6$ per group) (N). Scale bars: 0.2 mm (A), 1 mm (D), 0.3 mm (G and L) and 30 μm (H and M). $^*P < 0.05$ vs. PBS. Arrowheads (A and B) indicate microvessels at the border of the MCA and ACA cortex (red line). Arrows (L and N) indicate the border of infarcted tissue (left side, stroke MCA area; right side, viable ACA area).

immediate post-stroke period (up to 3 days), although there was a long-term effect on brain atrophy (evaluated at 35 days).

Granulocyte colony-stimulating factor enhances the inflammatory response after stroke

Further studies were performed to analyse the apparent dichotomy between G-CSF-mediated enhancement of neovascularization of the ischemic territory post-stroke vs. increased cerebral atrophy and lack of improvement in behavioral testing. We focused our studies on the inflammatory response. Compared with PBS-treated mice (Fig. 2G, lower magnification; Fig. 2H, higher magnification), increased accumulation of CD11b-positive inflammatory cells, including monocytes and granulocytes (Campanella *et al.*, 2002), was observed in G-CSF-treated mice (50 μg/kg) at the border of the infarcted area (Fig. 2I, lower magnification; Fig. 2J, higher magnification). Quantitative analysis ($n = 6$ each) revealed a significant difference in the number of infiltrating CD-11b-positive cells (Fig. 2K; $P < 0.05$). These results led us to evaluate the presence of activated macrophages/microglia in ischemic lesions, as the latter are known to enhance brain damage after stroke (Mabuchi *et al.*, 2000). Although F4/80$^+$ activated macrophages/microglia were observed in the viable (i.e. non-ischemic) ACA area following treatment with PBS (Fig. 2L, lower magnification; Fig. 2M, higher magnification), increased numbers of F4/80$^+$ macrophages/microglia were observed in post-stroke animals treated with G-CSF (Fig. 2N, lower magnification; Fig. 2O, higher magnification). F4/80$^+$ activated macrophages/microglia in post-stroke mice treated with PBS were principally limited to the area close to the border of the infarcted tissue. In contrast, F4/80$^+$ cells in post-stroke mice treated with G-CSF were observed in a broad area and at higher density in the ACA territory. The total number of F4/80$^+$ cells in a section at the exact center of the forebrain was quantified ($n = 6$ each); a significant increase in F4/80$^+$ activated macrophages/microglia was observed in G-CSF-treated mice, compared with controls receiving PBS post-stroke (Fig. 2P; $P < 0.05$).

Administration of granulocyte colony-stimulating factor 1 h after stroke also induces brain atrophy

As the experimental protocol for the above studies involved G-CSF treatment starting 24 h after stroke, it was important to vary our protocol. For this purpose, we also administered G-CSF within 1 h of stroke (Fig. 3A, $n = 6$ each) or performed continuous treatment for up to 7 days (Fig. 3B, $n = 6$ each). Our results demonstrate induction of brain atrophy in post-stroke animals treated with G-CSF subjected to either of these protocols compared with PBS-treated controls.

To exclude the immune response stimulated by human recombinant G-CSF in mice, various doses of mouse recombinant G-CSF were administered and the effect was determined ($n = 6$ each dose). We found significant brain atrophy with administration of lower doses (0.5 and 5 μg/kg) of recombinant murine G-CSF. As the survival rate was only 50% (three mice dead out of six) with administration of a higher dose (50 μg/kg), the group was excluded from this analysis.

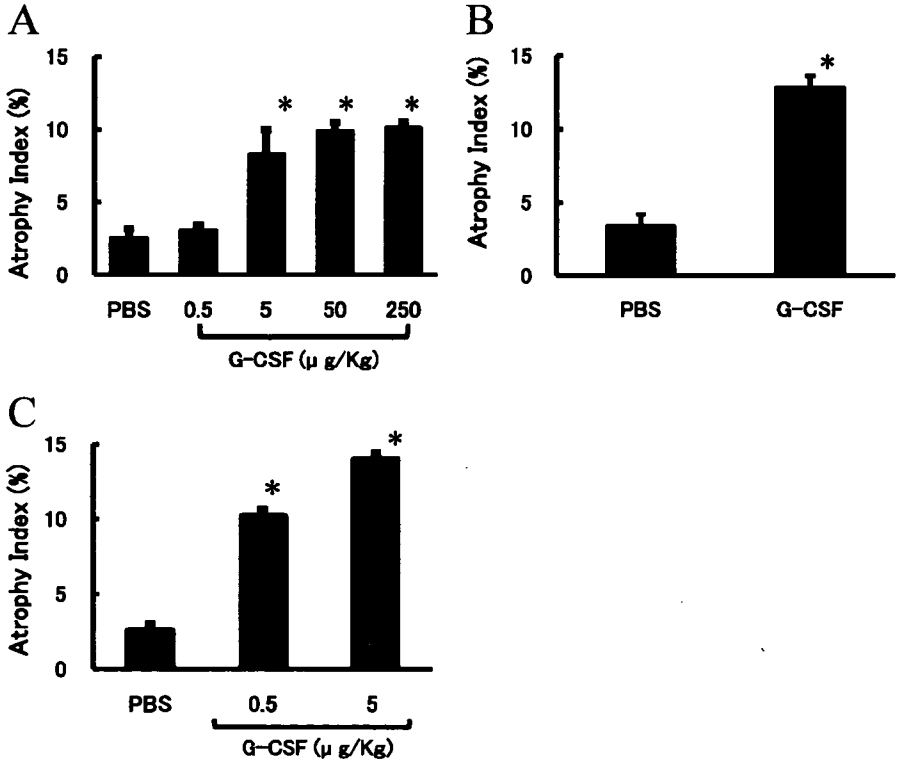

FIG. 3. Effect of granulocyte colony-stimulating factor (G-CSF) on brain atrophy. (A) G-CSF or phosphate-buffered saline (PBS) was administered 1 h after stroke and brains were evaluated grossly on day 35 post-stroke. (B) Continuous administration of G-CSF or PBS starting at 1 h post-stroke for 7 days was also tested. (C) Mouse recombinant G-CSF was administrated at the indicated dose and was found to increase the atrophy index. In each case, $n = 6$ per group. *$P < 0.05$ vs. PBS.

Discussion

Our results demonstrate that, in a murine permanent focal cerebral infarction model, administration of G-CSF, either human or murine recombinant, post-stroke is associated with enhanced brain atrophy.

In order to evaluate experimental treatments for stroke, reproducible induction of cerebral ischemia/infarction is a prerequisite: Previously, we developed a stroke model using SCID mice (Taguchi *et al.*, 2004) that proved suitable for quantification of the effect of cell therapy on neurogenesis, neovessel formation and neural function. In the current study, we have applied this stroke model to CB-17 mice and found it to provide highly reproducible data.

Granulocyte colony-stimulating factor is known to mobilize EPCs from bone marrow (Willing *et al.*, 2003) and accelerate angiogenesis (Bussolino *et al.*, 1991). Clinical studies have demonstrated that administration of G-CSF has beneficial effects in patients with acute myocardial infarction, including promotion of neovascularization and improvement of perfusion (Kuethe *et al.*, 2004). In addition, G-CSF has been shown to display neuroprotective properties in a rodent model (Schabitz *et al.*, 2003). Based on these observations, G-CSF has been tested in animal models of transient cerebral ischemia and beneficial effects have been reported (i.e. reduced infarct volume and enhanced functional recovery) (Schabitz *et al.*, 2003; Shyu *et al.*, 2004; Gibson *et al.*, 2005). In the current study, we employed a permanent cerebral infarction (i.e. stroke) model, rather than a model of transient ischemia, to investigate the effects of G-CSF.

In addition to its effects on EPCs, G-CSF is known to mobilize granuloctyes from the bone marrow, and these granulocytes have been shown to become associated with endothelia and accumulate in the ischemic brain (Justicia *et al.*, 2003). These observations suggested the possibility that G-CSF might augment the inflammatory response consequent to ischemic tissue damage by promoting recruitment and activation of neutrophils and mononuclear-derived cells (blood monocytes, monocyte-derived macrophages and microglia) (Zawadzka & Kaminska, 2005). Consistent with this concept, accumulation of CD11b-positive inflammatory cells at the border of the infarcted area was observed after treatment with G-CSF. Furthermore, a striking increase in the number of F4/80$^+$ activated macrophages/microglia was observed in non-ischemic surviving tissue (adjacent to the infarct) subsequent to administration of G-CSF. The inflammatory response after stroke has been shown to have both positive and negative effects on tissue repair (Fontaine *et al.*, 2002). Our results indicated that the balance of these inflammatory mechanisms on stroke outcome in the mouse using a permanent ischemia model and following administration of G-CSF is negative.

It would appear that the current work contradicts previous studies showing a positive effect of G-CSF after myocardial ischemia (Minatoguchi *et al.*, 2004). This apparent discrepancy may be explained, at least in part, by differences in brain and cardiac vasculature. Non-ischemic brain is protected from the systemic inflammatory response by an intact blood–brain barrier composed of endothelia joined by tight junctions. Thus, invasion of the central nervous system by activated inflammatory cells is largely prevented and the neural system functions within a relatively protected microenvironment, with respect to the inflammatory response (Neumann, 2000). However, stroke disturbs the integrity of the blood–brain barrier. We propose that a combination of impaired function of the blood–brain barrier in the context of G-CSF-induced augmentation of the inflammatory response in ischemic tissue contributes to the observed brain atrophy. Although activated inflammatory cells are known to participate in both the injurious and healing processes (Minatoguchi *et al.*, 2004), our results indicate an overall negative effect on neural function and neurogenesis following treatment with G-CSF in the post-stroke period.

In contrast to G-CSF, EPO had beneficial effects after stroke in the current model. Such positive effects are consistent with previous reports (Bernaudin *et al.*, 1999; Bahlmann *et al.*, 2004; Bartesaghi *et al.*, 2005; Kretz *et al.*, 2005) demonstrating that EPO promotes mobilization of EPCs (Bahlmann *et al.*, 2004), has angiogenic (Jaquet *et al.*, 2002) and neuroprotective properties (Bartesaghi *et al.*, 2005), and accelerates regeneration (Kretz *et al.*, 2005).

Taken together, our results indicate that administration of G-CSF after stroke results in an exaggerated inflammatory response, both at the border of the ischemic region and also in non-ischemic brain tissue, and that this is associated with brain atrophy and poor neural function. Thus, we suggest that a cautious approach should be taken in applying results of studies with G-CSF in the peripheral circulation (i.e. limb and cardiac ischemia) to the setting of cerebral ischemia. In a more general context, it is possible that agents with pro-inflammatory properties will prove less useful as therapeutic agents in cerebral ischemia in view of the above observations.

Acknowledgements

This work was partially supported by a Grant-in-Aid for Scientific Research from the Ministry of Health, Labour and Welfare. We would like to thank Y. Kasahara for technical assistance.

Abbreviations

ACA, anterior cerebral artery; EPC, endothelial progenitor cell; EPO, erythropoietin; F4/80$^+$, F4/80-positive; G-CSF, granulocyte colony-stimulating factor; MCA, middle cerebral artery; PBS, phosphate-buffered saline; SCID, severe combined immunodeficient; TTC, 2,3,5-triphenyltetrazolium.

References

Asahara, T., Murohara, T., Sullivan, A., Silver, M., van der Zee, R., Li, T., Witzenbichler, B., Schatteman, G. & Isner, J.M. (1997) Isolation of putative progenitor endothelial cells for angiogenesis. *Science*, **275**, 964–967.

Bahlmann, F.H., De Groot, K., Spandau, J.M., Landry, A.L., Hertel, B., Duckert, T., Boehm, S.M., Menne, J., Haller, H. & Fliser, D. (2004) Erythropoietin regulates endothelial progenitor cells. *Blood*, **103**, 921–926.

Bartesaghi, S., Marinovich, M., Corsini, E., Galli, C.L. & Viviani, B. (2005) Erythropoietin: a novel neuroprotective cytokine. *Neurotoxicology*, **26**, 923–928.

Bernaudin, M., Marti, H.H., Roussel, S., Divoux, D., Nouvelot, A., MacKenzie, E.T. & Petit, E: (1999) A potential role for erythropoietin in focal permanent cerebral ischemia in mice. *J. Cereb. Blood Flow Metab.*, **19**, 643–651.

Bussolino, F., Ziche, M., Wang, J.M., Alessi, D., Morbidelli, L., Cremona, O., Bosia, A., Marchisio, P.C. & Mantovani, A. (1991) In vitro and in vivo activation of endothelial cells by colony-stimulating factors. *J. Clin. Invest.*, **87**, 986–995.

Campanella, M., Sciorati, C., Tarozzo, G. & Beltramo, M. (2002) Flow cytometric analysis of inflammatory cells in ischemic rat brain. *Stroke*, **33**, 586–592.

Dzau, V.J., Gnecchi, M., Pachori, A.S., Morello, F. & Melo, L.G. (2005) Therapeutic potential of endothelial progenitor cells in cardiovascular diseases. *Hypertension*, **46**, 7–18.

Ehrenreich, H., Hasselblatt, M., Dembowski, C., Cepek, L., Lewczuk, P., Stiefel, M., Rustenbeck, H.H., Breiter, N., Jacob, S., Knerlich, F., Bohn, M., Poser, W., Ruther, E., Kochen, M., Gefeller, O., Gleiter, C., Wessel, T.C., De Ryck, M., Itri, L., Prange, H., Cerami, A., Brines, M. & Siren, A.L. (2002) Erythropoietin therapy for acute stroke is both safe and beneficial. *Mol. Med.*, **8**, 495–505.

Fontaine, V., Mohand-Said, S., Hanoteau, N., Fuchs, C., Pfizenmaier, K. & Eisel, U. (2002) Neurodegenerative and neuroprotective effects of tumor

necrosis factor (TNF) in retinal ischemia: opposite roles of TNF receptor 1 and TNF receptor 2. *J. Neurosci.*, **22**, RC216.

Gibson, C.L., Bath, P.M. & Murphy, S.P. (2005) G-CSF reduces infarct volume and improves functional outcome after transient focal cerebral ischemia in mice. *J. Cereb. Blood Flow Metab.*, **25**, 431–439.

Jaquet, K., Krause, K., Tawakol-Khodai, M., Geidel, S. & Kuck, K.H. (2002) Erythropoietin and VEGF exhibit equal angiogenic potential. *Microvasc. Res.*, **64**, 326–333.

Justicia, C., Panes, J., Sole, S., Cervera, A., Deulofeu, R., Chamorro, A. & Planas, A.M. (2003) Neutrophil infiltration increases matrix metalloproteinase-9 in the ischemic brain after occlusion/reperfusion of the middle cerebral artery in rats. *J. Cereb. Blood Flow Metab.*, **23**, 1430–1440.

Kimble, D.P. (1968) Hippocampus and internal inhibition. *Psychol. Bull.*, **70**, 285–295.

Kretz, A., Happold, C.J., Marticke, J.K. & Isenmann, S. (2005) Erythropoietin promotes regeneration of adult CNS neurons via Jak2/Stat3 and PI3K/AKT pathway activation. *Mol. Cell Neurosci.*, **29**, 569–579.

Kuethe, F., Figulla, H.R., Voth, M., Richartz, B.M., Opfermann, T., Sayer, H.G., Krack, A., Fritzenwanger, M., Hoffken, K., Gottschild, D. & Werner, G.S. (2004) Mobilization of stem cells by granulocyte colony-stimulating factor for the regeneration of myocardial tissue after myocardial infarction. *Dtsch. Med. Wochenschr.*, **129**, 424–428.

Mabuchi, T., Kitagawa, K., Ohtsuki, T., Kuwabara, K., Yagita, Y., Yanagihara, T., Hori, M. & Matsumoto, M. (2000) Contribution of microglia/macrophages to expansion of infarction and response of oligodendrocytes after focal cerebral ischemia in rats. *Stroke*, **31**, 1735–1743.

Matsushita, K., Matsuyama, T., Nishimura, H., Takaoka, T., Kuwabara, K., Tsukamoto, Y., Sugita, M. & Ogawa, S. (1998) Marked, sustained expression of a novel 150-kDa oxygen-regulated stress protein, in severely ischemic mouse neurons. *Brain Res. Mol. Brain Res.*, **60**, 98–106.

Minatoguchi, S., Takemura, G., Chen, X.H., Wang, N., Uno, Y., Koda, M., Arai, M., Misao, Y., Lu, C., Suzuki, K., Goto, K., Komada, A., Takahashi, T., Kosai, K., Fujiwara, T. & Fujiwara, H. (2004) Acceleration of the healing process and myocardial regeneration may be important as a mechanism of improvement of cardiac function and remodeling by postinfarction granulocyte colony-stimulating factor treatment. *Circulation*, **109**, 2572–2580.

Neumann, H. (2000) The immunological microenvironment in the CNS: implications on neuronal cell death and survival. *J. Neural Transm. Suppl.*, **59**, 59–68.

Schabitz, W.R., Kollmar, R., Schwaninger, M., Juettler, E., Bardutzky, J., Scholzke, M.N., Sommer, C. & Schwab, S. (2003) Neuroprotective effect of granulocyte colony-stimulating factor after focal cerebral ischemia. *Stroke*, **34**, 745–751.

Shyu, W.C., Lin, S.Z., Yang, H.I., Tzeng, Y.S., Pang, C.Y., Yen, P.S. & Li, H. (2004) Functional recovery of stroke rats induced by granulocyte colony-stimulating factor-stimulated stem cells. *Circulation*, **110**, 1847–1854.

Taguchi, A., Soma, T., Tanaka, H., Kanda, T., Nishimura, H., Yoshikawa, H., Tsukamoto, Y., Iso, H., Fujimori, Y., Stern, D.M., Naritomi, H. & Matsuyama, T. (2004) Administration of CD34+ cells after stroke enhances neurogenesis via angiogenesis in a mouse model. *J. Clin. Invest.*, **114**, 330–338.

Tamatani, M., Matsuyama, T., Yamaguchi, A., Mitsuda, N., Tsukamoto, Y., Taniguchi, M., Che, Y.H., Ozawa, K., Hori, O., Nishimura, H., Yamashita, A., Okabe, M., Yanagi, H., Stern, D.M., Ogawa, S. & Tohyama, M. (2001) ORP150 protects against hypoxia/ischemia-induced neuronal death. *Nat. Med.*, **7**, 317–323.

Walther, T., Olah, L., Harms, C., Maul, B., Bader, M., Hortnagl, H., Schultheiss, H.P. & Mies, G. (2002) Ischemic injury in experimental stroke depends on angiotensin II. *Faseb J.*, **16**, 169–176.

Wang, L., Zhang, Z., Wang, Y., Zhang, R. & Chopp, M. (2004) Treatment of stroke with erythropoietin enhances neurogenesis and angiogenesis and improves neurological function in rats. *Stroke*, **35**, 1732–1737.

Weaver, C.H., Buckner, C.D., Longin, K., Appelbaum, F.R., Rowley, S., Lilleby, K., Miser, J., Storb, R., Hansen, J.A. & Bensinger, W. (1993) Syngeneic transplantation with peripheral blood mononuclear cells collected after the administration of recombinant human granulocyte colony-stimulating factor. *Blood*, **82**, 1981–1984.

Willing, A.E., Vendrame, M., Mallery, J., Cassady, C.J., Davis, C.D., Sanchez-Ramos, J. & Sanberg, P.R. (2003) Mobilized peripheral blood cells administered intravenously produce functional recovery in stroke. *Cell Transplant.*, **12**, 449–454.

Zawadzka, M. & Kaminska, B. (2005) A novel mechanism of FK506-mediated neuroprotection: downregulation of cytokine expression in glial cells. *Glia*, **49**, 36–51.

ORIGINAL RESEARCH

Visualization of Intracerebral Arteries by Synchrotron Radiation Microangiography

K. Myojin
A. Taguchi
K. Umetani
K. Fukushima
N. Nishiura
T. Matsuyama
H. Kimura
D.M. Stern
Y. Imai
H. Mori

BACKGROUND AND PURPOSE: Small cerebral vessels are a major site for vascular pathology leading to cerebral infarction and hemorrhage. However, such small cerebral vessels are difficult to visualize by using conventional methods. The goal of our study was the development of methodology allowing visualization of small cerebral arteries in rodents, suitable for experimental models.

MATERIALS AND METHODS: Using barium sulfate as a contrast material, we obtained microangiographic images of physiologic and pathologic changes consequent to cerebral infarction in mouse brain by monochromatic synchrotron radiation (SR). To achieve high-resolution and high-contrast images, we used a new x-ray camera with a pixel size of 4.5 μm, and we set the energy level at 37.5 keV, just above the K absorption of barium.

RESULTS: Small intracerebral arteries (~30 μm in diameter) were clearly visualized, as well as the cortical branches (50–70 μm in diameter) at the brain surface. The limit of detection appeared to be vessels ~10 μm in diameter. Compared with the noninfarcted side, the number of intracerebral arteries was dramatically decreased in the middle cerebral artery area affected by stroke.

CONCLUSIONS: These results indicate the potential of SR for evaluating pathologic changes in small cerebral arteries and for monitoring the impact of pro- and antiangiogenic therapeutic strategies.

Cerebrovascular disease is one of the major causes of death and disability in developed countries. To evaluate cerebral vasculature, conventional angiography and MR angiography are commonly used in clinical practice. The development of these imaging methods has allowed analysis of the pathologic features of cerebrovascular lesions and has guided therapeutic strategies. However, small cerebral vessels, including those known to harbor causative lesions in cerebral infarction and hemorrhage (due to lipohyalinotic changes and/or microaneurysm formation),[1] such as intracerebral arteries and perforators, are below the detection limit of conventional imaging techniques. An important step in developing therapeutic strategies effective against disease in small cerebral vessels is enhanced visualization of this vasculature, especially in experimental models.

Recently, ex vivo and in vivo microangiography using monochromatic synchrotron radiation (SR) has been suggested as a tool capable of visualizing pathophysiologic changes in small arteries. Using this system has made possible the detection of microcirculation in the dermis,[2] tumors,[3] and collateral microvessels in ischemic hind limbs.[4] Although fluorescence microscopy has also been used to image small arteries,[5-7] SR imaging has the advantage of visualizing microvessels, even after they enter the parenchyma of an organ. In contrast, fluorescence techniques do not allow adequate visualization of small arteries once a vessel is deep within brain or other parenchymal tissue. On the basis of these observations, we have developed a microangiographic system using SR and have investigated physiologic and pathologic features of rodent cerebral microvasculature.

Received August 3, 2006; accepted after revision August 31.

From the Departments of Cerebrovascular Disease (K.M., A.T.) and Cardiac Physiology (K.F., N.N., H.M.), National Cardiovascular Center, Osaka, Japan; the Department of Radiology (K.M., Y.I.), Tokai University School of Medicine, Kanagawa, Japan; Japan Synchrotron Radiation Research Institute (K.U.), Hyogo, Japan; the Department of Internal Medicine (T.M.), Hyogo College of Medicine, Hyogo, Japan; Dainippon Sumitomo Pharma Co Ltd (H.K.), Osaka, Japan; and the Dean's Office (D.M.S.), College of Medicine, Cincinnati University, Cincinnati, Ohio.

Experiments were performed at the SPring-8 BL28B2 beamline with the approval of the Japan Synchrotron Radiation Research Institute (acceptance No. 2005B0359).

This work was partially supported by a Grant-in-Aid for Scientific Research from the Ministry of Health, Labor and Welfare and The New Energy and Industrial Technology Development Organization.

Please address correspondence to Akihiko Taguchi, MD, Department of Cerebrovascular Disease, National Cardiovascular Center, 5-7-1 Fujishiro-dai, Suita, Osaka, Japan, 565-8565; e-mail: Taguchi ataguchi@res.ncvc.go.jp

Materials and Methods

All procedures were performed in accordance with the National Cardiovascular Center Animal Care and Use Committee.

Preparation of Contrast Medium

For high-contrast images of the microcirculation, contrast agents included microspheres (Techpolymer I-2, Sekisui Plastics, Shiga, Japan) and barium sulfate (BarytgenSol, Fushimi, Tokushima, Japan). However, because the diameter of microspheres was 15 μm, whereas that of barium sulfate particles varied from 1–100 μm, the microcirculation of cerebral arteries could not be visualized by using these contrast media (not shown). To perfuse such microvessels (diameter <10 μm), we filtered barium sulfate (pore size 5 μm; Millex-SV, Millipore, Bedford, Mass) and obtained particles <5 μm in diameter. Filtered barium sulfate particles were then centrifuged (3000 G, 60 minutes) and concentrated to 50% by weight following removal of the supernatant.

Injection of Contrast Medium

Male severe combined immunodeficient (SCID) mice (6 weeks old; weight, 25–30 g; Oriental Yeast, Tokyo, Japan) were anesthetized by using inhaled diethyl ether and were perfused systemically with phosphate-buffered saline (PBS) containing heparin (40 U/mL) via the left ventricle of the heart with a peristaltic pump (Iwaki, Asahi Techno Glass, Chiba, Japan). Filtered barium sulfate particles (<5 μm in diameter, prepared as described previously; 50% by weight) were infused (0.7 mL), followed by isolation of the brain and fixation in formalin.

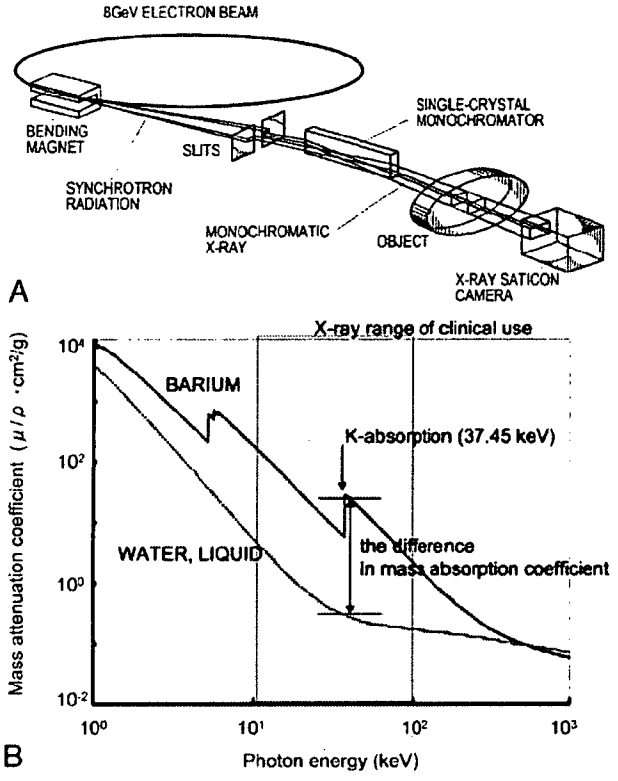

Fig 1. Schematic depiction of the monochromatic SR system. *A*, Illustration of the experimental arrangement for SR microangiography at BL28B2. *B*, Photon mass attenuation coefficient of barium (*blue line*) and liquid water (*red line*). Monochromatic x-ray energy is adjusted to 37.5 keV, just above the barium K-edge energy to produce the highest contrast image.

Microangiography and Image Analysis

Microangiographic images of mouse brain were obtained by using monochromatic SR in the Japan Synchrotron Radiation Research Institute (SPring-8, Hyogo, Japan).[4,8] There are 3 large 3rd-generation synchrotron radiation facilities in the world: the Advanced Photon Source in Argonne (United States), the European Synchrotron Radiation Facility in Grenoble (France), and SPring-8 (the latter was used for the studies described herein). These facilities are open to scientists in many fields, including material, chemical, and life sciences investigators. The experimental setup for x-ray imaging by using monochromatic SR at the SPring-8 BL28B2 beamline is shown in Fig 1*A*. The storage ring was operated at 8-GeV electron beam energy, and beam current was 80–100 mA. The distance between the point source in the bending magnet and the detector was ~45 m. A nearly parallel x-ray beam was used for imaging without blurring because of the small size of the x-ray source and the very long source-to-object distance. The single crystal monochromator selects a single energy of synchrotron radiation. The shutter system is located between the monochromator and the object. X-rays transmitted through the object are detected by an x-ray direct-conversion-type detector incorporating the x-ray saticon pickup tube. Monochromatic x-ray energy was adjusted to 37.5 keV, just above the barium K-edge energy, to produce the highest contrast image of the barium (Fig 1*B*). X-ray flux at the object position was around 1×10^{10} photons/mm^2 per second in imaging experiments. The images were acquired as 1024 × 1024 pixels with 10-bit resolution after analog-to-digital conversion. The FOV was 4.5 × 4.5 mm^2, and pixel size was ~4.5 μm.[9,10]

Mammographic Images

To compare spatial and contrast resolution, we obtained mammographic images, which are known for having the highest resolution in clinical applications,[11] of murine brains. Digital images were captured at an energy level of 24 kV by using a molybdenum target and a molybdenum filter with 90° cranial projection. Source-to-image distance was 65 cm.

Induction of Focal Cerebral Ischemia

Permanent focal cerebral infarction was induced by ligation and disconnection of the left MCA of male SCID mice (n = 5), as described.[12–14] Briefly, under inhaled halothane (3%) anesthesia, animals were placed on their right sides and a skin incision was made at the midpoint between the left orbit and the external auditory canal. The temporalis muscle was incised, and the zygomatic arch was removed to expose the squamous portion of the temporal bone. Using a dental drill, we made a small hole above the distal portion, M1, of the MCA, which could be seen through the exposure in the skull. The dura mater was opened, and the left MCA was electrocauterized and disconnected just distal to its crossing of the olfactory tract. Body temperature was maintained at 36.5°–37°C by using a heat lamp during the operation and for 2 hours after MCA occlusion. Cerebral blood flow (CBF) in the left MCA area was measured by laser-Doppler flowmetry (Advance, Tokyo, Japan). The holding device of the laser probe (ALF probe; Neuroscience, Osaka, Japan) (1.5 mm in diameter, 7.0 mm in length) was secured on the cranium at a site located above the ischemic core of the left MCA area (approximately 1 mm anterior and 5 mm distal to the bregma), and CBF was monitored during the procedure and 24 hours after ligation of the MCA. Mice displaying a decrease in CBF by ~75% immediately after the procedure and thereafter for an additional 24 hours were used for experiments.[15] Nine days after induction of cerebral ischemia, the cerebral microcirculation was examined by SR imaging.

MR Imaging System

To confirm cerebral infarction consequent to ligation of the MCA, we performed MR imaging on day 2 poststroke. MR imaging used a 2T compact MR imaging system with a permanent magnet (MRmini SA206, Dainippon Sumitomo Pharma, Osaka, Japan) by using a radio-frequency solenoid coil for signal-intensity detection. For each imaging sequence, 15 coronal images were acquired with a section thickness of 1 mm, gapped at 0.5 mm. T1-weighted spin-echo MR images were acquired with a TR/TE of 500/9 ms, a FOV of 36.6 × 18.3 mm, an image acquisition matrix of 256 × 128, and NEX, 4. T2-weighted spin-echo MR images were obtained with TR/TE, 3000/69, 256 × 128, and NEX, 2. Because the sequences to obtain diffusion-weighted images by using this machine are still in development, we evaluated the cerebral ischemia by T2-weighted images on day 2 poststroke.

Data Analysis

In all experiments, the mean ± SE is reported.

Results

Visualization of Cerebral Arteries by SR Imaging

After euthanasia and systemic perfusion with PBS, barium sulfate particles were infused via the left ventricle of the heart. As shown in Fig 2*A*, cerebral arteries on the brain surface were filled with contrast medium. First, we investigated vascular

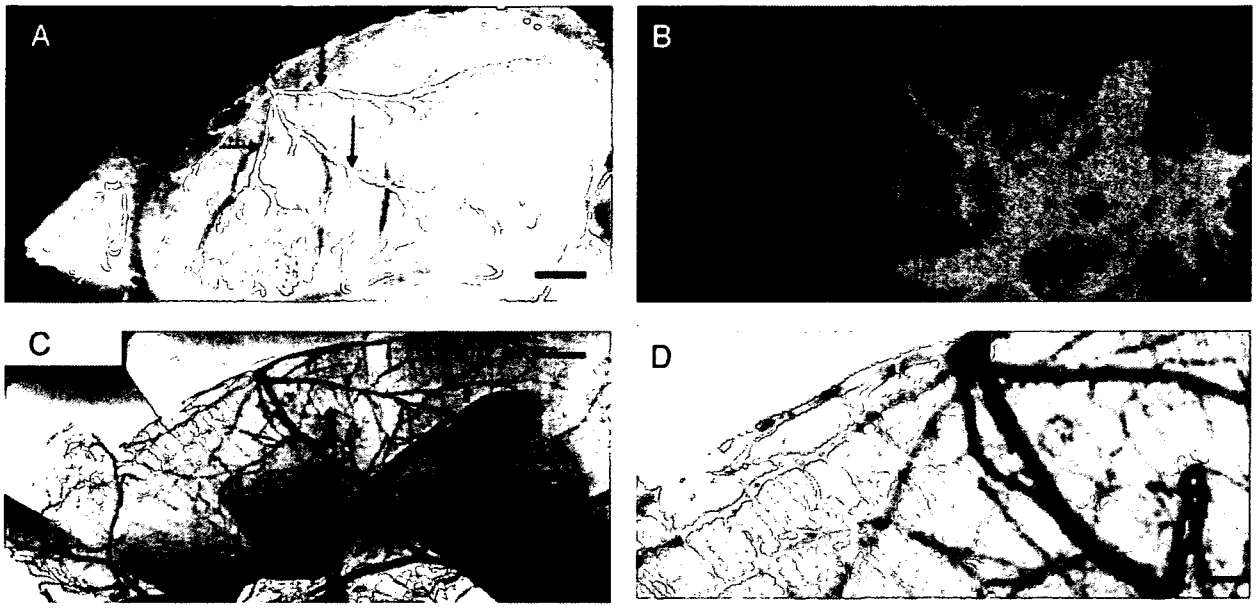

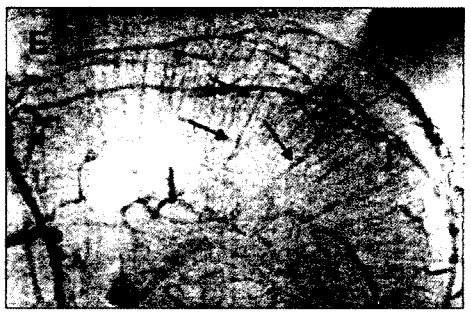

Fig 2. Angiographic image of mouse cerebral artery. *A*, Macroimage of the right brain hemisphere. The cerebral arteries (*arrows*), but not cerebral veins, are filled with the barium sulfate. *B*, Cerebral microangiogram (90° caudal projection) with a mammographic soft x-ray machine. Mammography enables visualization of small cerebral arteries and penetrating intracerebral arteries, but the image is not sufficient to evaluate pathologic changes. *C* and *D*, Cerebral angiograms obtained by SR. Note that small cerebral vessels, including penetrating intracerebral arteries, are clearly visualized. Microvascular structures, such as orthogonal branching of penetrating intracerebral arteries from the cortical artery, are clearly observed by the enlarged SR imaging (*D*). *E*, Coronal section of a cerebral microangiogram. Two distinct penetrating intracerebral arteries, superficial penetrating arteries and deep penetrating arteries (*arrow*), are clearly observed by the SR image. Scale bars: 1 mm (*A* and *B*), 0.5 mm (*C* and *E*), and 250 μm (*D*).

images by mammography (Fig 2*B*). However, sufficient spatial and contrast resolution was not obtained by mammographic imaging to evaluate the angioarchitecture of small cerebral vasculature. Peripheral branches of the MCA (75–100 μm in diameter) and small vessels emerging from peripheral branches were barely visualized.

Next, we investigated the vascular profile by using SR (Fig 2*C*, normal view; -*D*, enlarged view). At the brain surface, cortical arteries branching from the MCA and pial arteries, ~30 μm in diameter, were clearly visualized. Within the brain parenchyma, penetrating intracerebral arteries, branching orthogonally from cortical or pial arteries, were also observed. The interval between intracerebral arteries was 126.1 ± 35.5 μm (n = 20), the diameter of the proximal side of the intracerebral arteries was 29.5 ± 3.1 μm (n = 20), and each intracerebral artery was observed to progressively narrow to a diameter below the limit of resolution (10 μm). Vascular diameters determined by SR imaging of intracerebral arteries and small arterial branches were identical to those observed in previous pathologic studies of murine brain.[16] Using SR imaging, we could discern 2 types of intracerebral arteries: superficial penetrating arteries perfusing only the cortical area and penetrating arteries reaching the subcortical area and perfusing the deep white matter. These vascular structures observed in murine brain by SR imaging are similar to previous observations in human anatomic studies.[17-20] Compared with mammographic images, SR imaging enabled visualization of penetrating intracerebral arteries (diameter range of 10–30 μm), as well as small peripheral branches of MCA at the brain surface, with remarkable clarity. Using a coronal view for cerebral microangiograms, we also discerned 2 distinct penetrating arteries, superficial and deep (Fig 2*E*).

SR Images after Cerebral Infarction

To evaluate cerebral vasculature in the context of pathologic changes, cerebral infarction was induced by ligation of the MCA. The area of cerebral infarction was visualized by MR imaging on day 2 after induction of stroke. As we have shown previously by 2,3,5-triphenyltetrazolium staining,[12] limited cortical infarction was observed in the MCA area on T2-weighted images (Fig 3*A*). In contrast, no hyper- or hypointense region was observed on T1-weighted images (Fig 3*B*), indicating the absence of bleeding or parenchymal injury. Although no morphologic (Fig 3*C*) or vascular structural (Fig 3*D*) changes were observed in the right hemisphere (nonstroke side), by day 9 after MCA occlusion, tissue degradative changes were observed in the cortical and shallow white matter of the left MCA area (stroke side, Fig 3*E*). To evaluate the integrity of the microvasculature after stroke, we obtained SR images. The number of penetrating intracerebral arteries dramatically decreased, though cortical branches at the brain surface could still be visualized (Fig 3*F*). On the coronal view, the disappearance of the intracerebral arteries on the ischemic side was also clearly observed (Fig 3*G*).

Discussion

Cerebral artery disease in small vessels is a major cause of cerebral infarction and hemorrhage. Although pathologic changes in small arteries have been reported on the basis of microscopic analysis, it has been difficult to assess the mor-

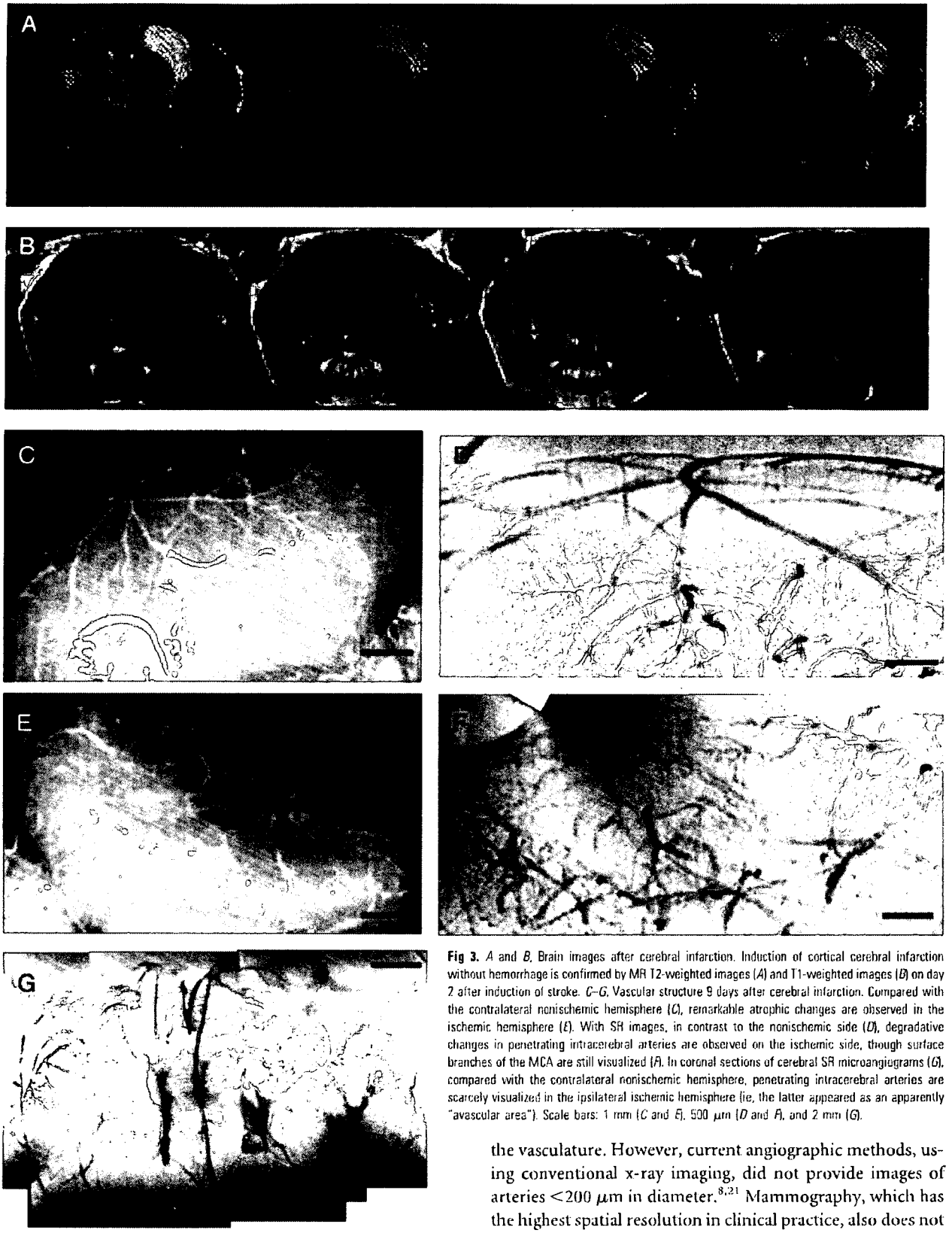

Fig 3. *A* and *B*, Brain images after cerebral infarction. Induction of cortical cerebral infarction without hemorrhage is confirmed by MR T2-weighted images (*A*) and T1-weighted images (*B*) on day 2 after induction of stroke. *C–G*, Vascular structure 9 days after cerebral infarction. Compared with the contralateral nonischemic hemisphere (*C*), remarkable atrophic changes are observed in the ischemic hemisphere (*E*). With SR images, in contrast to the nonischemic side (*D*), degradative changes in penetrating intracerebral arteries are observed on the ischemic side, though surface branches of the MCA are still visualized (*F*). In coronal sections of cerebral SR microangiograms (*G*), compared with the contralateral nonischemic hemisphere, penetrating intracerebral arteries are scarcely visualized in the ipsilateral ischemic hemisphere (ie, the latter appeared as an apparently "avascular area"). Scale bars: 1 mm (*C* and *E*), 500 μm (*D* and *F*), and 2 mm (*G*).

phology of small cerebral vessels in situ through imaging studies. Herein, we demonstrate that small cerebral vessels can be clearly visualized by microangiography by using SR.

Conventional angiography is commonly used to evaluate the vasculature. However, current angiographic methods, using conventional x-ray imaging, did not provide images of arteries <200 μm in diameter.[8,21] Mammography, which has the highest spatial resolution in clinical practice, also does not have sufficient resolution to visualize small vessels with a diameter of <50 μm.[11] Microangiographic techniques have been developed by using fine-focus x-rays and sensitive films to evaluate the microcirculation in the brain.[20] These methods enable visualization of human cortical perforating arteries and

medullary long branches (100 μm in diameter) by using 1-cm-thick sections of brain.[20] However, the limit of detection by using these methods applied to thick sections has been reported to be vessels of 50 μm in diameter.[22] Furthermore, visualization of smaller arteries required thin sections cut with a microtome.[20] The latter method is not well-suited to the evaluation of 3D cerebral vascular trees.

Compared with these conventional methods, the principal advantage of SR is the small size of the electron beam, thereby providing a high-intensity x-ray point source. Using a nearly parallel beam of SR, along with a precise detection system (pixel size of 4.5 μm), allowed us to obtain high-quality angiographic images with excellent spatial resolution. Furthermore, setting SR at an energy level just above the K absorption of barium produced the highest contrast images. SR imaging provides a powerful tool to reveal the morphology of small cerebral arteries such as superficial and deep penetrating arteries, allowing analysis of their physiologic and pathologic properties under a variety of conditions (ie, borderzone in infarction[23,24] and microaneurysm formation).

Fluorescence microscopy is another tool potentially useful for analysis of the microcirculation.[25] Although fluorescence microscopy provides visualization of microcirculation at the brain surface, the advantage of SR imaging is visualization of small vessels that have penetrated into the brain parenchyma, such as the subcortex. In addition, SR imaging allows performance of microangiography with an optimal projection. When the latter is combined with a microinjector, sequential real-time images can be obtained, providing the substrate for hemodynamic analysis.

In this article, we investigated SR imaging after stroke and showed that the SR image reflects pathologic changes previously observed by using anatomic/microscopic analysis. On day 9 after MCA occlusion, arteries on the surface of the cerebrum were visualized by SR, though penetrating intracerebral arteries were not detected. Previous studies have shown that the integrity of the distal cortical artery is usually maintained after occlusion of the proximal artery and that collateral flow is established through expansion of previously existing and/or formation of new vascular channels.[25,26] Analysis with enhanced MR imaging has shown cerebral parenchymal enhancement in the stroke area by 1 week after cerebral infarction,[27] indicative of blood flow in the peri-ischemic area. In contrast, penetrating intracerebral arteries were dramatically decreased in number in the ischemic hemisphere, though cortical branches on the brain surface were maintained after MCA occlusion. It has previously been shown that microvasculature in the ischemic territory displays adhesion of polymorphonuclear leukocytes in postcapillary venules, followed by the disruption of the microvascular network.[28] These previous findings are consistent with the results of our vascular images obtained by SR after ligation of the MCA.

Conclusion

Our study demonstrates, for the first time, the morphologic features of small vascular networks in murine brain by microangiography by using SR imaging. Our approach provides a powerful tool for evaluating potential angiogenic/antiangiogenic therapeutic strategies, as well as pathologic examination of the cerebral microarterial tree.

Acknowledgments

We thank Y. Kasahara, K. Tomiyasu, and M. Aoki for technical assistance.

References

1. Phillips SJ, Whisnant JP. **Hypertension and the brain: The National High Blood Pressure Education Program.** *Arch Intern Med* 1992;152:938–45
2. Ito K, Tanaka E, Mori H, et al. **A microangiographic technique using synchrotron radiation to visualize dermal circulation in vivo.** *Plast Reconstr Surg* 1998;102:1128–33
3. Tokiya R, Umetani K, Imai S, et al. **Observation of microvasculatures in athymic nude rat transplanted tumor using synchrotron radiation microangiography system.** *Academic Radiology* 2004;9:1039–46
4. Takeshita S, Isshiki T, Mori H, et al. **Use of synchrotron radiation microangiography to assess development of small collateral arteries in a rat model of hindlimb ischemia.** *Circulation* 1997;95:805–08
5. Conway JG, Popp JA, Thurman RG. **Microcirculation in periportal and pericentral regions of lobule in perfused rat liver.** *Am J Physiol* 1985;249:G449–56
6. Stock RJ, Cilento EV, McCuskey RS. **A quantitative study of fluorescein isothiocyanate-dextran transport in the microcirculation of the isolated perfused rat liver.** *Hepatology* 1989;9:75–82
7. Birngruber R, Schmidt-Erfurth U, Teschner S, et al. **Confocal laser scanning fluorescence topography: a new method for three-dimensional functional imaging of vascular structures.** *Graefes Arch Clin Exp Ophthalmol* 2000;238:559–65
8. Mori H, Hyodo K, Tanaka E, et al. **Small-vessel radiography in situ with monochromatic synchrotron radiation.** *Radiology* 1996;201:173–77
9. Umetani K, Yagi N, Suzuki Y, et al. **Observation and analysis of microcirculation using high-spatial-resolution image detectors and synchrotron radiation.** *Proceeding of SPIE* 2000;3977:522–33
10. Yamashita T, Kawashima S, Ozaki M, et al. **Images in cardiovascular medicine: mouse coronary angiograph using synchrotron radiation microangiography.** *Circulation* 2002;105:E3–4
11. Kuzmiak CM, Pisano ED, Cole EB, et al. **Comparison of full-field digital mammography to screen-film mammography with respect to contrast and spatial resolution in tissue equivalent breast phantoms.** *Med Phys* 2005;32:3144–50
12. Taguchi A, Soma T, Tanaka H, et al. **Administration of CD34+ cells after stroke enhances neurogenesis via angiogenesis in a mouse model.** *J Clin Invest* 2004;114:330–38
13. Furuya K, Kawahara N, Kawai K, et al. **Proximal occlusion of the middle cerebral artery in C57Black6 mice: relationship of patency of the posterior communicating artery, infarct evolution, and animal survival.** *J Neurosurg* 2004;100:97–105
14. Kitagawa K, Matsumoto M, Mabuchi T, et al. **Deficiency of intercellular adhesion molecule 1 attenuates microcirculatory disturbance and infarction size in focal cerebral ischemia.** *J Cereb Blood Flow Metab* 1998;18:1336–45
15. Matsushita K, Matsuyama T, Nishimura H, et al. **Marked, sustained expression of a novel 150-kDa oxygen-regulated stress protein, in severely ischemic mouse neurons.** *Brain Res Mol Brain Res* 1998;60:98–106
16. Coyne EF, Ngai AC, Meno JR, et al. **Methods for isolation and characterization of intracerebral arterioles in the C57/BL6 wild-type mouse.** *J Neurosci Methods* 2002;120:145–53
17. Herman LH, Ostrowski AZ, Gurdjian ES. **Perforating branches of the middle cerebral artery: an anatomical study.** *Arch Neurol* 1963;8:32–34
18. Kaplan HA. **The lateral perforating branches of the anterior and middle cerebral arteries.** *J Neurosurg* 1965;23:305–10
19. de Reuck J. **The area of the deep perforating branches of the median cerebral artery in man [in French].** *Acta Anat (Basel)* 1969;74:30–35
20. Salamon G, Combalbert A, Faure J, et al. **Microradiographic study of the arterial circulation of the brain.** *Prog Brain Res* 1968;30:33–41
21. Mori H, Hyodo K, Tobita K, et al. **Visualization of penetrating transmural arteries in situ by monochromatic synchrotron radiation.** *Circulation* 1994;89:863–71
22. Salamon G, Raybaud C, Michotey P, et al. **Angiographic study of cerebral convolutions and their area of vascularization [in French].** *Rev Neurol (Paris)* 1975;131:259–84
23. Bogousslavsky J, Regli F. **Centrum ovale infarcts: subcortical infarction in the superficial territory of the middle cerebral artery.** *Neurology* 1992;42:1992–98
24. Donnan GA, Norrving B, Bamford JM, et al. **Subcortical infarctions: classification and terminology.** *Cerebrovasc Dis* 1993;3:248–51
25. Tomita Y, Kubis N, Calando Y, et al. **Long-term in vivo investigation of mouse cerebral microcirculation by fluorescence confocal microscopy in the area of focal ischemia.** *J Cereb Blood Flow Metab* 2005;25:858–67
26. Zulch KJ. *Cerebral Circulation and Stroke.* Berlin, Germany: Springer-Verlag; 1971:116
27. Merten CL, Knitelius HO, Assheuer J, et al. **MRI of acute cerebral infarcts: increased contrast enhancement with continuous infusion of gadolinium.** *Neuroradiology* 1999;41:242–48
28. del Zoppo GJ, Mabuchi T. **Cerebral microvessel responses to focal ischemia.** *J Cereb Blood Flow Metab* 2003;23:879–94